Eur. Phys. J. C (2025) 85:183
https://doi.org/10.1140/epjc/s10052-025-13858-y

THE EUROPEAN PHYSICAL JOURNAL C

Regular Article -Theoretical Physics

$f(Q)$ gravitational theory and its structure via redshift

G. G. L. Nashed[1,2,a]

[1] Centre for Theoretical Physics, The British University in EGypt, P.O. Box 43, El Sherouk City, Cairo 11837, Egypt
[2] Center for Space Research, North-West University, Potchefstroom 2520, South Africa

Received: 9 November 2024 / Accepted: 19 January 2025

Abstract We introduce a new technique for reformulating the $f(Q)$ gravitational theory based on parameterization of the deceleration parameter or other options. This tool allows us to create modified gravitational scenarios connected to cosmological observations. We examine two models of the deceleration parameter and one model of the effective equation of the state of the universe as discussed in the literature. We utilize the asymptotic behavior of the matter density parameter to further constrain the feasible range of the model parameters. One of the tested models shows how a tiny modification can produce viable cosmic scenarios quantitatively similar to ΛCDM but qualitatively different, whereas the dark energy (DE) sector becomes dynamic and fully explained by modified gravity, not by a cosmological constant.

1 Introduction

Penrose and Hawking introduced the energy condition (EC) in classical general relativity to explain the singularity caused by gravitational collapse while adhering to non-negativity of local energy and considering the causal structure of the universe [1–6]. Conventional matter does not match the observed evidence for the universe's accelerated expansion [7,8], prompting the need for alternative energy known as dark energy. These model-independent evaluations all concur that dark energy, characterized by negative effective pressure, is the dominant component of the current cosmic matter. Regrettably, all efforts to detect dark energy in the universe through physical means have been unsuccessful. This has resulted in the development of different gravity theories involving curvature. f(R) gravity, f(R, T) gravity, f(R, G) gravity, and similar theories have been proposed to address these issues through geometric interpretations rather than relying on the dark sector [9]. Albert Einstein himself introduced the metric teleparallel equivalent of general relativity (TEGR) that has been extensively researched, with the Levi–Civita connection being substituted by a teleparallel connection based on torsion. A new theory in metric teleparallelism called f(𝕋) theory was proposed to address the dark sector [10–12]. Another type of teleparallel theory, known as symmetric teleparallelism, can be found in the existing literature [13]. The focus of this study is on the recently introduced $f(Q)$ theories of gravity in symmetric teleparallelism, aiming to avoid dependencies on dark energy as proposed in [14].

Einstein GR is the conventional gravitational theory, which relies on curvature and the Einstein–Hilbert action [15]. However, it is understood that gravity can also be represented in alternative ways, such as the torsional and non-metricity formulations, specifically with the TEGR [16] and symmetric teleparallel equivalent of general relativity (STEGR) [13,14], respectively. Combined, these three identical expressions make up the geometric trio of gravity [17]. Changes in the curvature-based GR theory result in the popular f(R) gravity, f(G) gravity, Lovelock gravity, etc., as shown in [18–21]. Additionally, f(𝕋) gravity, an extension of TEGR, has been thoroughly examined and researched within the field of cosmology [22–29]. Ultimately, adjustments involving the non-metricity scalar Q, such as expansions of the STEGR, result in f(Q) gravity [14,30]. The cosmological implications of f(Q) gravity are quite fascinating, hence sparking a substantial amount of recent research [31–72].

In recent years, there have been several significant publications focusing on the f(Q) gravity theory and its implications for cosmology [31–36,48,52,73–90] and references therein. The corresponding ECs were also discussed [91,92]. Nevertheless, apart from Subramaniam et al. [92], all prior research has been conducted exclusively within the spatially flat Friedmann–Lemaitre–Robertson–Walker (FLRW) model of the universe, with the line element specifically using Cartesian coordinates. In this case, the f(Q) theory, known as

[a] e-mail: nashed@bue.edu.eg (corresponding author)

Published online: 14 February 2025

the coincident gauge choice, was developed utilizing a vanishing affine connection. The entire equation became simpler in this specific reference frame because the covariant derivative changed into a partial derivative. Nevertheless, we had to make a trade-off by ensuring that f(Q) theory and f($\mathbb{T}$) theory were in alignment, resulting in matching Friedmann equations for pressure and energy density [93]. In a previous study [92], an analysis of this problem is discussed by including a nonzero affine connection, but the analysis was still conducted within the context of a spatially flat FLRW spacetime.

As successful explanations of the universe's evolution would need to transition from deceleration to acceleration in accordance with observations, it is logical to characterize the late accelerated expansion using the deceleration parameter $q(z)$. Characterizing the late accelerated expansion by the deceleration parameter $q(z)$ is reasonable, as successful explanations of the universe's evolution should shift from deceleration to acceleration based on observations [94–106]. Nevertheless, this method fails to offer a rationale for the nature of dark energy. The majority of cosmological studies assume that the observable universe is spatially flat, meaning $k = 0$. Nevertheless, k must be limited whenever the most recent observational data is accessible. Hence, it would be ideal to consider the inclusion of the spatial curvature k. Some recent studies have thoroughly examined the impact of spatial curvature [107–114]. Studying the f(Q) theory in both open and closed FLRW models with $k = \pm 1$ is undeniably beneficial. Until the study by Dimakis et al. [115], the primary difficulty was the intricate mathematical formalism of symmetric teleparallelism in a background spacetime, with little effort made to show a clear formulation in both open and closed FLRW modes. The goal of this study is to place this kinematic method in the context of a revised theory of gravity that can be further tested at the perturbation level. A Big Bang nucleosynthesis formalism and observations were used in the framework of f(Q) theory to extract constraints on it [116]. They show [116] that f(Q) gravity can safely pass the Big Bang nucleosynthesis constraints which are not satisfied by some modified theories of gravity. The use of Hubble data and Gaussian processes to reconstruct the dynamical connection function in f(Q) cosmology beyond the coincident gauge is investigated in [74]; they show that in both cases, and according to the Akaike information criterion (AIC) and Bayesian information criterion (BIC), the inclusion of the non-coincident gauge is favored relative to the Λ-cold dark matter (CDM) paradigm.

This article is structured as follows: Following the introduction, Sect. 2 explains the fundamental mathematical framework of f(Q) theory, while Sect. 3 discusses the derivation of f(Q) from a nonzero affine connection in a spatially curved FLRW universe (positively and negatively curved). Such connection coefficients involve a heretofore unconstrained function of time, $\gamma(t)$. The Friedmann-like equations of energy and pressure for ordinary matter and the effective counterparts are also provided. The corresponding modifications of Friedmann equations of $f(Q)$ theory in cosmological applications are presented in Sect. 4. In Section 5, we demonstrate how the field equation of $f(Q)$ theory aligns with the deceleration parameter, enabling an effective methodology for reconstructing $f(Q)$ gravity. In Sect. IV, we utilize our reconstruction technique to derive the $f(Q)$ gravity framework that replicates the ΛCDM model. Moreover, we analyze two distinct parameterizations of the deceleration parameter within the context of their corresponding $f(Q)$ theories. Additionally, we explore a specific parametric form of the effective Equation of State (EoS) detailed in reference [117]. We then proceed to discuss the findings of each of these three models in detail. In conclusion, we provide a summary of the paper in Sect. 7.

2 An overview of symmetric teleparallelism

The theory of symmetric teleparallel gravity was constructed using an affine connection, $\Gamma^{\alpha}{}_{\beta\gamma}$, which is considered general and defined as follows:

$$\Gamma^{\lambda}{}_{\mu\nu} = \mathring{\Gamma}^{\lambda}{}_{\mu\nu} + L^{\lambda}{}_{\mu\nu}. \tag{1}$$

In the symmetric teleparallelism theory, gravity is governed by the non-metricity of the underlying geometry, which has no curvature and zero torsion. The first step is to establish the definition of the non-metricity tensor that has the form

$$\mathrm{Q}_{\lambda\mu\nu} = \nabla_{\lambda} g_{\mu\nu}. \tag{2}$$

There are two potential traces for the non-metricity tensor, which are defined as follows:

$$\mathrm{Q}_{\lambda} = Q_{\lambda\mu\nu} g^{\mu\nu}, \quad \tilde{Q}_{\nu} = Q_{\lambda\mu\nu} g^{\lambda\mu}.$$

The tensors $L^{\lambda}{}_{\mu\nu}$ and $P^{\lambda}{}_{\mu\nu}$ define the disformation and the superpotential, respectively, as follows:

$$\mathrm{L}^{\lambda}{}_{\mu\nu} = \frac{1}{2}(Q^{\lambda}{}_{\mu\nu} - Q_{\mu}{}^{\lambda}{}_{\nu} - Q_{\nu}{}^{\lambda}{}_{\mu}), \tag{3}$$

$$\mathrm{P}^{\lambda}{}_{\mu\nu} = \frac{1}{4}\left(-2L^{\lambda}{}_{\mu\nu} + Q^{\lambda} g_{\mu\nu} - \tilde{Q}^{\lambda} g_{\mu\nu} - \frac{1}{2}\delta^{\lambda}_{\mu} Q_{\nu} - \frac{1}{2}\delta^{\lambda}_{\nu} Q_{\mu}\right). \tag{4}$$

We are examining the scalar quantity of non-metricity, which has the form

$$\begin{aligned} \mathrm{Q} &= Q_{\lambda\mu\nu} P^{\lambda\mu\nu} \\ &= \frac{1}{4}(2Q_{\lambda\mu\nu} Q^{\mu\lambda\nu} - Q_{\lambda\mu\nu} Q^{\lambda\mu\nu} + Q_{\lambda} Q^{\lambda} - 2Q_{\lambda}\tilde{Q}^{\lambda}). \end{aligned} \tag{5}$$

However, like GR, symmetric teleparallelism also encounters the challenging issue known as the "dark" problem. Therefore, a modified $f(Q)$ gravity theory has been proposed, similar to the introduction of modified $f(R)$ theory, to expand upon GR. The action of this modified gravitational theory is given by

$$\mathrm{S} = \frac{1}{2\kappa}\int f(Q)\sqrt{-g}\,d^4x + \int \mathcal{L}_M\sqrt{-g}\,d^4x, \tag{6}$$

where $f(Q)$ is an arbitrary function of the non-metricity scalar, i.e., Q. Variation of Eq. (6) w.r.t. the metric yields the equation of motion as follows [14]:

$$\mathrm{f}_Q\mathring{G}_{\mu\nu} + \frac{1}{2}g_{\mu\nu}(f_Q Q - f) + 2f_{QQ}P^{\lambda}{}_{\mu\nu}\mathring{\nabla}_\lambda Q = \kappa T^m_{\mu\nu}, \tag{7}$$

where $\mathring{\mathrm{G}}_{\mu\nu}$ is the Einstein tensor. Now let us transform Eq. (7) into an equivalent form of GR as

$$\mathring{G}_{\mu\nu} = \frac{\kappa T^{eff}_{\mu\nu}}{f_Q} = \frac{\kappa T^m_{\mu\nu}}{f_Q} + T^{DE}_{\mu\nu}, \tag{8}$$

where

$$\mathrm{T}^{DE}_{\mu\nu} = \frac{1}{\kappa f_Q}\left[\frac{1}{2}g_{\mu\nu}(f - Qf_Q) - 2f_{QQ}\mathring{\nabla}_\lambda Q P^{\lambda}_{\mu\nu}\right] \tag{9}$$

refers to the extra terms resulting from the geometric alteration of the theory of gravity in this case. This can be easily imagined as the element that functions as a sort of imaginary dark force.

3 Homogeneous and isotropic model in the frame of $f(Q)$

The metric for an FLRW spacetime with spatial curvature and isotropic homogeneity is defined as

$$ds^2 = -dt^2 + R(t)^2\left(\frac{dr^2}{1-kr^2} + r^2d\theta^2 + r^2\sin^2\theta d\phi^2\right), \quad \text{where} \quad k = \pm 1, \tag{10}$$

where $\mathrm{R}(t)$ is the scale factor. In the frame of this spacetime, the compatible connection was deliberated in [115] as

$$\Gamma^t{}_{tt} = -\frac{\mathrm{k}+\dot{\mathrm{P}}}{\gamma}, \quad \Gamma^t{}_{rr} = \frac{\gamma}{1-\mathrm{kr}^2},$$
$$\Gamma^t{}_{\theta\theta} = \gamma r^2, \quad \Gamma^t{}_{\phi\phi} = \gamma r^2\sin^2\theta, \quad \Gamma^r{}_{tr} = -\frac{\mathrm{k}}{\gamma},$$
$$\Gamma^r{}_{rr} = \frac{\mathrm{kr}}{1-\mathrm{kr}^2}, \quad \Gamma^r{}_{\theta\theta} = -(1-kr^2)r,$$
$$\Gamma^r{}_{\phi\phi} = -(1-kr^2)r\sin^2\theta, \quad \Gamma^\theta{}_{t\theta} = -\frac{k}{\gamma},$$
$$\Gamma^\theta{}_{r\theta} = \frac{1}{\mathrm{r}}, \quad \Gamma^\theta{}_{\phi\phi} = -\cos\theta\sin\theta,$$
$$\Gamma^\phi{}_{t\phi} = -\frac{\mathrm{k}}{\gamma}, \quad \Gamma^\phi{}_{r\phi} = \frac{1}{r}, \quad \Gamma^\phi{}_{\theta\phi} = \cot\theta, \tag{11}$$

where $\gamma \equiv \gamma(t)$. The non-metricity scalar Q can be determined by using Eq. (5):

$$\mathrm{Q}(t) = -3\left[2H^2 + \left(\frac{3k}{\gamma} - \frac{\gamma}{R^2}\right)H - \frac{2k}{R^2} - k\frac{\dot{\gamma}}{\gamma^2} - \frac{\dot{\gamma}}{R^2}\right]. \tag{12}$$

Now let us examine regular matter that behaves like a perfect fluid, with its stress–energy tensor $\mathrm{T}^m_{\alpha\beta}$ given as

$$\mathrm{T}^m_{\alpha\beta} = (p^m + \rho^m)u_\alpha u_\beta + p^m g_{\alpha\beta}, \tag{13}$$

where u^μ is the fluid four-velocity unit vector. The Friedmann–Robertson–Walker (FRW) equations can be derived from the field equation (7), which gives

$$\rho^m = \frac{1}{2}f + \left(3H^2 + 3\frac{k}{R^2} - \frac{1}{2}Q\right)f_Q + \frac{3}{2}\dot{Q}\left(-\frac{k}{\gamma} - \frac{\gamma}{R^2}\right)f_{QQ}, \tag{14}$$

$$\mathrm{p}^m = -\frac{1}{2}f + \left(-3H^2 - 2\dot{H} - \frac{k}{R^2} + \frac{1}{2}Q\right)f_Q + \dot{Q}\left(-2H - \frac{3}{2}\frac{k}{\gamma} + \frac{1}{2}\frac{\gamma}{R^2}\right)f_{QQ}, \tag{15}$$

where the symbols p^m and ρ^m represent the pressure and energy density, respectively. The total energy density and pressure yield the form

$$\rho^{Tot} = \rho^m + \frac{1}{2}(Qf_Q - f) + \frac{3}{2}\dot{Q}f_{QQ}\left(\frac{\gamma}{R^2} + \frac{k}{\gamma}\right) \tag{16}$$

$$\mathrm{p}^{Tot} = p^m - \frac{1}{2}(Qf_Q - f) - \frac{1}{2}\dot{Q}f_{QQ}\left(\frac{\gamma}{R^2} - \frac{3k}{\gamma} - 4H\right), \tag{17}$$

where $\dot{\mathrm{Q}} \equiv \frac{dQ}{dt}$, $\mathrm{f}_Q \equiv \frac{\partial f}{\partial Q}$, $\mathrm{f}_{QQ} \equiv \frac{\partial^2 f}{\partial Q^2}$.

4 Analysis focused on a particular model

In this section, we consider the extension of GR in terms of $f(Q)$. In spherical coordinates, with the line element given by (10) and spatial curvature $k = 0$, we set $\gamma(t) = 0$ [115]. Inserting Eq. (10) into the field equations (7) and by making

use of the useful relation (12), the FRW equations can be expressed in terms of $f(Q)$ as[1]

$$\rho^m = \frac{1}{2\kappa}(\mathrm{f} - \mathrm{Hf_H}),$$
$$\mathrm{p}^m = -\frac{1}{2\kappa}\left(\mathrm{f} - \mathrm{Hf_H} - \frac{1}{3}\dot{\mathrm{H}}\mathrm{f_{HH}}\right) \equiv \frac{1}{6\kappa}\dot{\mathrm{H}}\mathrm{f_{HH}} - \rho^{\mathrm{m}}, \quad (18)$$

where $\mathrm{f_Q} = \frac{df}{dQ} \equiv -\frac{f_H}{12H}$ with $\mathrm{f_H} = \frac{\mathrm{df}}{\mathrm{dH}}$ similar for $\mathrm{f_{QQ}} = \frac{d^2f}{dQ^2}$ with $\mathrm{f_{HH}} = \frac{d^2f}{dH^2}$.

To close the system, it is necessary to select an equation of state (EoS) to link ρ^m and p^m. For the simplest barotropic case $\mathrm{p^m} \equiv \mathrm{p^m}(\rho^{\mathrm{m}}) = \mathrm{w_m}\rho^{\mathrm{m}}$, the above system produces the useful dynamical equation

$$\dot{\mathrm{H}} = 3(1 + \mathrm{w_m})\left[\frac{\mathrm{f(H)} - \mathrm{Hf_H}}{\mathrm{f_{HH}}}\right] = \mathrm{F(H)}. \quad (19)$$

As is evident from the previous relation, $\dot{H}$ is dependent solely on H, so Eq. (19) describes the phase portrait of any $\mathrm{f}(Q)$ gravity in a flat FRW background. This study examines the later stages of cosmic evolution, assuming a universe predominantly made up of baryons with $w_m = 0$ before transitioning to dark energy dominance.

Due to the impressive outcomes observed in general relativity, modified gravity theories should be acknowledged as adjustments to it. It is beneficial to express the field equations in a manner that incorporates Einstein's gravity along with correction terms from the higher order of $\mathrm{f}(Q)$ symmetric teleparallel gravity. Therefore, we express the amended FRW equations as

$$\mathrm{H}^2 = \frac{\kappa}{3}\left(\rho^m + \rho^Q\right) \equiv \frac{\kappa}{3}\rho^{\mathrm{Tot}}, \quad (20)$$
$$2\dot{H} + 3H^2 = -\kappa\left(p^m + p^Q\right) \equiv -\kappa\mathrm{p}^{\mathrm{Tot}}. \quad (21)$$

In this scenario, the pressure and energy density of the symmetric teleparallel of $\mathrm{f}(Q)$ are determined by

$$\rho^Q(H) = \frac{1}{2\kappa}\left(\mathrm{Hf_H} - \mathrm{f(H)} + 6\mathrm{H}^2\right), \quad (22)$$
$$\mathrm{p}^Q(H) = -\frac{1}{6\kappa}\dot{\mathrm{H}}\,(12 + \mathrm{f_{HH}}) - \rho^{\mathrm{Q}}(\mathrm{H}). \quad (23)$$

When $\mathrm{f(Q)} = Q$, which is the GR limit, then ρ^Q and p^Q are both equal to zero. In cases in which $\mathrm{f}(Q)$ is not linear, the non-metricity scalar Q corresponding to $\mathrm{f}(Q)$ may act as the dark energy. In the barotropic situation, the non-metricity scalar will possess an equation of state as

$$\omega_{DE} = \omega_Q(H) = -1 - \frac{1}{3}\frac{\dot{H}(12 + f_{HH})}{6H^2 - f(H) + Hf_H}. \quad (24)$$

[1] Equations (19) reduce to the symmetric teleparallel equivalent of GR when $f(Q) \equiv Q$.

The density parameters $w_i = \frac{\rho_i}{\rho_c}$ are defined, with i denoting the species component and ρ_c the critical density ($\equiv \rho^{Tot}$). Therefore, the dimensionless version of the FRW equation (20) is expressed as

$$\mathrm{w_m} + \mathrm{w_Q} = 1, \quad (25)$$

with w_m being the matter density parameter, calculated as $\frac{\kappa\rho^{\mathrm{m}}}{3\mathrm{H}^2}$, while w_Q is the non-symmetric density parameter, calculated as $\frac{\kappa\rho_Q}{3H^2}$. In order to uphold the conservation law, the continuity equations are obtained by minimally coupling the matter field and the non-symmetric:

$$\dot{\rho}^{\mathrm{m}} + 3\mathrm{H}\rho^{\mathrm{m}} = 0, \quad (26)$$
$$\dot{\rho}^{\mathrm{Q}} + 3\mathrm{H}(\rho^{\mathrm{Q}} + \mathrm{p^Q}) = 0. \quad (27)$$

Defining the total EoS parameter can also be beneficial, and in this case it takes the form

$$\omega^{Tot} \equiv \frac{p^{Tot}}{\rho_{Tot}} = -1 - \frac{2}{3}\frac{\dot{H}}{H^2}. \quad (28)$$

The total EoS parameter may serve as a substitute for the deceleration parameter q, as they are connected as

$$\mathrm{q} \equiv -1 - \frac{\dot{\mathrm{H}}}{\mathrm{H}^2} = \frac{1}{2}\left(1 + 3\omega^{Tot}\right). \quad (29)$$

Multiple cosmological observations confirm that the universe transitioned from slowing to accelerating its expansion a few billion years ago. Since that time, the deceleration parameter q has been commonly utilized to characterize the evolution of the universe up to the present moment. In this way, certain individuals have employed various parametric forms of q [94–99,102], while others utilized non-parametric versions of q [100,101,103–106]. Nevertheless, these requirements must be defined within the context of a theory of gravity. In the following section, we demonstrate the method for reconstructing $\mathrm{f}(Q)$ gravity based on a specified form of $\mathrm{q}(z)$, where z represents the redshift, or other parameters like $\mathrm{w^{Tot}(z)}$. This enables us to conduct additional tests on the free parameters of these forms using other cosmological parameters such as the matter density parameter w_m or the dark energy equation of state.

5 Method for reconstructing $\mathrm{f}(Q)$ in symmetric teleparallel theory

Using the redshift z as the independent variable is practical, defined as $z = \frac{R_0}{R} - 1$, with $R_0 = 1$ at the current time. In this scenario, we put down

$$\dot{\mathrm{H}} = -(1 + \mathrm{z})\mathrm{HH}', \quad (30)$$

where the prime represents the derivative with respect to the redshift parameter z. By utilizing Eqs. (29) and (30), we can express $\mathrm{H}(z)$ as

$$\mathrm{H}(z) = H_0 \exp\left(\int_0^z \frac{1+q(\tilde{z})}{1+\tilde{z}} d\tilde{z}\right), \tag{31}$$

where H_0 is equal to H at redshift $\mathrm{z} = 0$. On the contrary, if we utilize z as the independent variable, then we obtain

$$\mathrm{f}(H(z)) = f(z), \quad \mathrm{f}_H = \frac{f'}{H'}, \quad \mathrm{f}_{HH} = \frac{f''H' - f'H''}{H'^3}. \tag{32}$$

By inserting Eqs. (30) and (32) into the phase portrait $\mathrm{f}(Q)$ described in Eq. (19), we can evaluate $H(z)$ as

$$\mathrm{H}(z) = H_0 \exp\left(\int_0^z \frac{f'(\tilde{z})}{f(\tilde{z}) + f_0(1+\tilde{z})^3} d\tilde{z}\right), \tag{33}$$

with f_0 being a constant that is incorporated into the equation. By inserting Eqs. (30) and (32) into Eq. (18), we determine the density of the matter as a function of the redshift as

$$\rho^{\mathrm{m}}(\mathrm{z}) = \frac{1}{2\kappa}\left(\mathrm{f}(\mathrm{z}) - \frac{\mathrm{H}}{\mathrm{H}'}\mathrm{f}'\right) = -\frac{\mathrm{f}_0}{2\kappa}(1+\mathrm{z})^3. \tag{34}$$

Alternatively, one can calculate the matter density by solving the matter continuity Eq. (26), where $\rho^m = \frac{\rho_{m,0}}{R^3} = \rho_{m,0}(1+z)^3$, with $\rho_{m,0}$ being the present matter density. By contrasting with Eq. (34), we find that $f_0 = -2\kappa\rho_{m,0}$. Currently ($\mathrm{z} = 0$), we have $w_{m,0} = \frac{\rho_{m,0}}{\rho_{c,0}} = \frac{\kappa\rho_{m,0}}{3H_0^2}$, which results in

$$\mathrm{f}_0 = -6\mathrm{w}_{\mathrm{m},0}\mathrm{H}_0^2. \tag{35}$$

The Planck cosmic microwave background (CMB) results show that $w_{m,0}h^2 = 0.1426 \pm 0.0020$ when using the ΛCDM model with Planck TT+lowP likelihood, where $h = H_0/100$ km/s/Mpc [118]. This immediately sets the constant's value as $f_0 = -8556$.

The relationship between the deceleration parameter $\mathrm{q}(\mathrm{z})$ and the modified $\mathrm{f}(\mathrm{Q})$ gravity with the Hubble function $\mathrm{H}(\mathrm{z})$ is similar according to Eqs. (31) and (33). Therefore, when we contrast these, we get

$$\mathrm{q}(\mathrm{z}) = \frac{(1+\mathrm{z})\mathrm{f}'}{\mathrm{f}(\mathrm{z}) - 6\mathrm{w}_{\mathrm{m},0}\mathrm{H}_0^2(1+\mathrm{z})^3} - 1. \tag{36}$$

The deceleration parameter is directly linked to the nature of the cosmic expansion rate, as mentioned previously. Therefore, various parameterization forms of the deceleration have been proposed in research to depict the cosmic evolution [94–106]. Thus, it can be concluded that Eq. (36) serves as a resource for creating feasible cosmic scenarios in the framework of $\mathrm{f}(Q)$ gravitational theory.

Instead, Eq. (36) can be used in the integration to derive $\mathrm{f}(\mathrm{z})$ as

$$\mathrm{f}(\mathrm{z}) = -6\mathrm{w}_{\mathrm{m},0}\mathrm{H}_0^2 \mathrm{e}^{\int_0^{\mathrm{z}} \frac{1+\mathrm{q}(\tilde{\mathrm{z}})}{1+\tilde{\mathrm{z}}} \mathrm{d}\tilde{\mathrm{z}}} \int_0^{\mathrm{z}} \frac{(1+\tilde{\mathrm{z}})^2(1+\mathrm{q}(\tilde{\mathrm{z}}))}{\mathrm{e}^{\int_0^{\mathrm{z}} \frac{1+\mathrm{q}(\tilde{\mathrm{z}})}{1+\tilde{\mathrm{z}}} \mathrm{d}\tilde{\mathrm{z}}}} \mathrm{d}\tilde{\mathrm{z}}. \tag{37}$$

Therefore, with a specific parameterization of $\mathrm{q}(\mathrm{z})$, Eq. (37) allows for the creation of the corresponding $\mathrm{f}(Q)$ theory, followed by the calculation and comparison of other key parameters with observational data to assess the credibility of $\mathrm{f}(\mathrm{Q})$ theory. In the present study, Eq. (37) is employed to analyze the $\mathrm{f}(\mathrm{Q})$ gravitational theory and its associated parameterization $\mathrm{q}(\mathrm{z})$. Furthermore, we can swap $\mathrm{q}(\mathrm{z})$ with $\mathrm{w}^{\mathrm{Tot}}(\mathrm{z})$ using (29), allowing for the reconstruction of $\mathrm{f}(\mathrm{Q})$ gravity with various parameterizations of $\mathrm{w}^{\mathrm{Tot}}(\mathrm{z})$ as well. In this case, we encounter an alternative reconstruction equation as

$$\begin{aligned}\mathrm{f}(\mathrm{z}) \; &= -9\mathrm{w}_{\mathrm{m},0}\mathrm{H}_0^2 \mathrm{e}^{\frac{3}{2}\int_0^{\mathrm{z}} \frac{1+\mathrm{w}^{Tot}(\tilde{\mathrm{z}})}{1+\tilde{\mathrm{z}}} \mathrm{d}\tilde{\mathrm{z}}} \\ &\times \int_0^{\mathrm{z}} \frac{(1+\tilde{\mathrm{z}})^2(1+\mathrm{w}^{Tot}(\tilde{\mathrm{z}}))}{\mathrm{e}^{\frac{3}{2}\int_0^{\mathrm{z}} \frac{1+\mathrm{w}_{eff}(\tilde{\mathrm{z}})}{1+\tilde{\mathrm{z}}} \mathrm{d}\tilde{\mathrm{z}}}} \mathrm{d}\tilde{\mathrm{z}}.\end{aligned} \tag{38}$$

To include additional reconstruction techniques, we consider scenarios where parameterizations are provided for the EoS of the dark energy sector. By substituting Eqs. (30) and (32) into Eq. (24), we get

$$\omega_{\mathrm{Q}}(\mathrm{z}) = -1 + \frac{1}{3}(1+\mathrm{z})\mathrm{H}\frac{12\mathrm{H}'^3 + \mathrm{f}''\mathrm{H}' - \mathrm{f}'\mathrm{H}''}{(6\mathrm{H}^2 - \mathrm{f})\mathrm{H}'^2 + \mathrm{H}\mathrm{H}'\mathrm{f}'}. \tag{39}$$

Equation (39) can be employed to recreate $\mathrm{f}(\mathrm{z})$ using a specified parameterization of the dark energy EoS $\mathrm{w}_{\mathrm{Q}}(\mathrm{z})$. By substituting Eq. (33) into Eq. (39), we can obtain a novel formulation given by

$$\omega_{\mathrm{Q}}(\mathrm{z}) = \frac{\left[\mathrm{f}(\mathrm{z}) - 6\mathrm{w}_{\mathrm{m},0}\mathrm{H}_0^2(1+\mathrm{z})^3 - \frac{2}{3}(1+\mathrm{z})\mathrm{f}'(\tilde{\mathrm{z}})\right]\mathrm{e}^{2\int_0^{\mathrm{z}} \frac{\mathrm{f}'(\tilde{\mathrm{z}})}{\mathrm{f}(\tilde{\mathrm{z}}) - 6\mathrm{w}_{\mathrm{m},0}\mathrm{H}_0^2(1+\tilde{\mathrm{z}})^3} \mathrm{d}\tilde{\mathrm{z}}}}{\left[\mathrm{f}(\mathrm{z}) - 6\mathrm{w}_{\mathrm{m},0}\mathrm{H}_0^2(1+\mathrm{z})^3\right]\left[\mathrm{w}_{\mathrm{m},0}(1+\mathrm{z})^3 - \mathrm{e}^{2\int_0^{\mathrm{z}} \frac{\mathrm{f}'(\tilde{\mathrm{z}})}{\mathrm{f}(\tilde{\mathrm{z}}) - 6\mathrm{w}_{\mathrm{m},0}\mathrm{H}_0^2(1+\tilde{\mathrm{z}})^3} \mathrm{d}\tilde{\mathrm{z}}}\right]}. \tag{40}$$

By inserting Eqs. (31) and (37) into Eq. (39), we discover a valuable connection between the dark energy equation of state and the deceleration parameter as

$$\omega_{\mathrm{Q}}(\mathrm{z}) = \frac{(1 - 2\mathrm{q}(\mathrm{z}))\,\mathrm{e}^{2\int_0^{\mathrm{z}} \frac{1+\mathrm{q}(\tilde{\mathrm{z}})}{1+\tilde{\mathrm{z}}} \mathrm{d}\tilde{\mathrm{z}}}}{3\left(\mathrm{w}_{\mathrm{m},0}(1+\mathrm{z})^3 - \mathrm{e}^{2\int_0^{\mathrm{z}} \frac{1+\mathrm{q}(\tilde{\mathrm{z}})}{1+\tilde{\mathrm{z}}} \mathrm{d}\tilde{\mathrm{z}}}\right)}. \tag{41}$$

Once more, we can use $q(z)$ and $\omega^{Tot}(z)$ mutually using Eq. (29). This allows us to establish a relationship between the dark energy and the total equation of state parameters as

$$\omega_{\mathrm{Q}}(\mathrm{z}) = -\frac{\omega^{Tot}(\mathrm{z})\mathrm{e}^{3\int_0^{\mathrm{z}}\frac{1+\mathrm{w_{eff}}(\tilde{\mathrm{z}})}{1+\tilde{\mathrm{z}}}\mathrm{d}\tilde{\mathrm{z}}}}{\mathrm{w_{m,0}}(1+\mathrm{z})^3 - \mathrm{e}^{3\int_0^{\mathrm{z}}\frac{1+\omega_{Tot}(\tilde{\mathrm{z}})}{1+\tilde{\mathrm{z}}}\mathrm{d}\tilde{\mathrm{z}}}}. \tag{42}$$

To conclude this section, we establish a connection between the deceleration parameter and another essential cosmological parameter, which enables the examination of assumed forms of $q(z)$ through the matter density parameter $\mathrm{w_m(z)}$. Using (34), we write

$$\mathrm{w_m(z)} = \frac{\mathrm{fH'} - \mathrm{Hf'}}{6\mathrm{H'H}^2} = \mathrm{w_{m,0}}(1+\mathrm{z})^3\,\mathrm{e}^{-2\int_0^{\mathrm{z}}\frac{1+\mathrm{q}(\tilde{\mathrm{z}})}{1+\tilde{\mathrm{z}}}\mathrm{d}\tilde{\mathrm{z}}}. \tag{43}$$

Furthermore, the dark symmetric teleparallel counterpart is subsequently provided by

$$\mathrm{w_Q} = 1 - \mathrm{w_m} = 1 - \mathrm{w_{m,0}}(1+\mathrm{z})^3\,\mathrm{e}^{-2\int_0^{\mathrm{z}}\frac{1+\mathrm{q}(\tilde{\mathrm{z}})}{1+\tilde{\mathrm{z}}}\mathrm{d}\tilde{\mathrm{z}}}. \tag{44}$$

In the next part, we will utilize these equations to investigate various parametric forms in f(Q) gravity.

6 Applications

Inspired by the results obtained in Sect. 5, we introduce three distinct parameterizations, two for the deceleration parameter q(z) and one for the effective EoS parameter $\omega^{\mathrm{Tot}}(\mathrm{z})$, with the objective of formulating the corresponding f(Q) gravity theory and exploring potential deviations from the ΛCDM model.

6.1 The flat model of ΛCDM

The dark energy scenario is one method used to explain the late accelerated expansion phase. A straightforward approach is to connect it to a cosmological constant through which the cosmic expansion shifts from slowing to accelerating, known as ΛCDM cosmology, aligning well with various observations. Nevertheless, the model lacks theoretical explanations and validation. In this framework, the evolution of the Hubble parameter is presented as

$$\mathrm{H(z)} = \mathrm{H_0}\sqrt{\mathrm{w_{m,0}}(1+\mathrm{z})^3 + \mathrm{w_{\lambda,0}}}\,, \tag{45}$$

where $w_{\lambda,0}$ represents $1 - w_{m,0}$, which indicates the current value of the dark energy density parameter. By plugging Eq. (45) into Eq. (29) and considering Eq. (30), we express the deceleration parameter for ΛCDM as

$$\mathrm{q(z)} = \frac{3}{2}\frac{\mathrm{w_{m,0}}(1+\mathrm{z})^3}{\mathrm{w_{\lambda,0}} + \mathrm{w_{m,0}}(1+\mathrm{z})^3} - 1. \tag{46}$$

At high redshifts, when $(1+\mathrm{z})^3$ is much greater than $\frac{\mathrm{w_{\lambda,0}}}{\mathrm{w_{m,0}}}$, the model displays a decelerating expansion phase similar to the Einstein–de Sitter model, where q approaches 1/2. Nevertheless, at low redshifts, the expansion transitions to an accelerating phase as q(z) decreases, then progresses towards pure de Sitter $\mathrm{q} \to -1$ as $\mathrm{z} \to -1 (\mathrm{t} \to \infty)$. Therefore, this form presents a feasible cosmological model that aligns with observations. Furthermore, by substituting Eq. (46) into Eq. (37), we can determine the relevant f(Q) gravity representation as

$$\mathrm{f(z)} = -6\mathrm{H_0^2}\left(\mathrm{w_{m,0}}(1+\mathrm{z})^3 + \mathrm{w_{\lambda,0}}\right) - 6\mathrm{w_{\lambda,0}}\mathrm{H_0^2}. \tag{47}$$

As anticipated, this results in $\mathrm{f(Q)_{\Lambda CDM}} = \mathrm{Q} - \mathrm{const.}$, specifically in the ΛCDM model [119]. Therefore, observations are necessary to constrain the two parameters of the model: $\mathrm{H_0}$ and $\Omega_{\mathrm{m,0}}$. Actually, the CMB and baryonic acoustic oscillation (BAO) data in the local region, assuming the ΛCDM model, support $\mathrm{H_0} = 68$ km/s/Mpc and $\Omega_{\mathrm{m,0}} = 0.3$, whereas the type I supernova (SNIa) and global $\mathrm{H_0}$ data (independent of model) prefer a higher $\mathrm{H_0} = 73$ km/s/Mpc and lower $\Omega_{\mathrm{m,0}} = 0.26$. Nevertheless, various methods have been proposed to harmonize local and global observations, such as incorporating dark neutrino species [120] or implementing dynamic phantom dark energy [121,122]. In the context of modified gravity, one can seek an explanation for the accelerated expansion without relying on dark energy (cosmological constant), but significant deviations from the ΛCDM model are not likely.

6.2 First application

Numerous different ways to parameterize the deceleration parameter have been proposed in various studies; however, they typically share a similar structure, given by

$$\mathrm{q(z)} = \mathrm{q_0} + \mathrm{q_1 X(z)}. \tag{48}$$

The datasets can determine the values of q_0 and q_1 provided they are real, but the function $X(z)$ can yield different representations of the deceleration parameter. Inspired by the parameterization of the dark energy of EoS presented in [123], a parameterization of the deceleration parameter that is free of divergences was proposed in [124]:

$$\mathrm{X(z)} = \frac{\mathrm{z}(1+\mathrm{z})}{1+\mathrm{z}^2}. \tag{49}$$

At high redshift $\mathrm{z} \gg 1$, the deceleration parameter $q(z)$ approaches $q_0 + q_1$, making it appropriate for analyzing

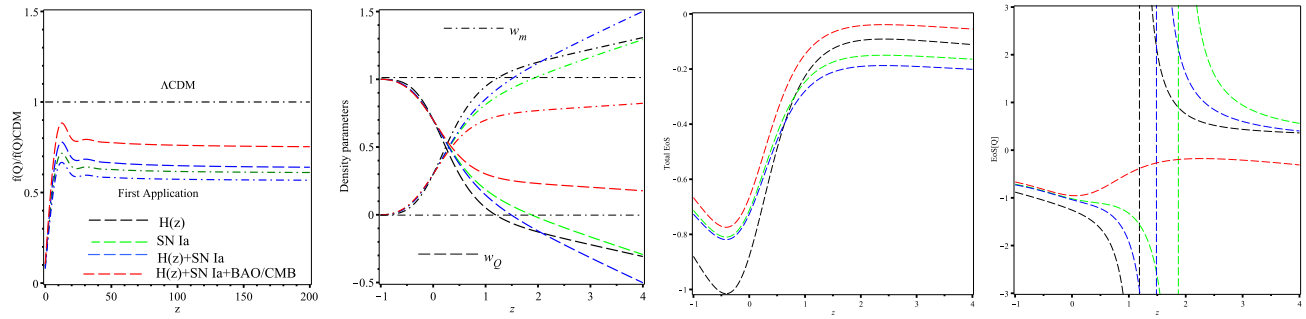

(a) $f(Q)$ theory (b) $w_m(z)$, $w_Q(z)$ behaviors (c) ω^{Tot} (d) ω_Q behavior

Fig. 1 The optimal values for the first application parameters [q_0, q_1] derived from [124] and based on the combinations of datasets used in that study. These values are $(-0.82,\ 0.98)$ for the H(z) dataset, $(-0.57,\ 0.70)$ for the SNIa dataset, $(-0.59,\ 0.67)$ for the combination of the SNIa and H(z) datasets, and $(-0.5,\ 0.78)$ for the combination of the SNIa, H(z), and BAO/CMB datasets. **a** The behavior of f(Q(z)) gravity normalized to ΛCDM. **b** The matter density parameter reaches 1 at redshifts between 1 and 2 for the H(z), SNIa, and SNIa + H(z) datasets. **c** The total EoS which is different from the standard cold dark matter model when $\omega^{\rm Tot} \to 0$ for redshifts $z \gtrsim 3$. To have a credible theory, it is anticipated to display fluctuations around ΛCDM. Since the theory does not align with ΛCDM, a viable thermal history is not anticipated in reality. **d** The symmetric teleparallel dark energy of EoS undergoes a phase transition in the redshift range of 1–2, with ω_Q approaching infinity for H(z), SNIa, and SNIa + H(z) datasets; for SNIa + H(z) + BAO/CMB datasets, it diverges at around $z \sim 10.3$. The labels used in panel **a** of this figure are the same as in panels **b–d**

the radiation era. In the late universe with $0 \le z \ll 1$, q(z) can be represented as the linear parametric expression $q(z) = q_0 + q_1 z$, making it appropriate to investigate the late accelerated expansion stage. In addition, it has been proven that q(z) remains finite as z approaches -1, making it appropriate for examining the universe's destiny. The parametric form given above is limited for every redshift $z \in [-1, \infty)$, making it suitable for depicting the entire cosmic timeline as noted in [124]. By utilizing the parametric Eqs. (49) and (31), the relation between Hubble and redshift can be formulated as

$$H(z) = H_0(1+z)^{1+q_0}(1+z^2)^{\frac{q_1}{2}}. \tag{50}$$

Furthermore, through the utilization of Eq. (37), we derive the form of f(z) that governs the gravity sector as

$$f(z) = -6w_{m,0}H_0^2(1+z)^{1+q_0}(1+z^2)^{\frac{q_1}{2}} \times \int_0^z \frac{1+q_0+q_1\frac{\tilde{z}(1+\tilde{z})}{1+\tilde{z}^2}}{(1+\tilde{z})^{q_0-1}(1+\tilde{z}^2)^{\frac{q_1}{2}}} d\tilde{z}. \tag{51}$$

Figure 1a displays the $f(Q)$ gravity results as a function of redshift for various q_0 and q_1 parameters. Figure 1a indicates significant discrepancies between the theory and the ΛCDM model, which is not commonly accepted. This should be evident in dynamic cosmological factors such as the matter density parameter.

Next, we assess the overall EoS parameter based on the parameterizations (49). Following Eq. (29), we have the expression

$$\omega^{\rm Tot}(z) = -1 + \frac{2}{3}\frac{(1+q_0)+q_1 z+(1+q_0+q_1)z^2}{1+z^2}. \tag{52}$$

By utilizing the parameterizations given in Eq. (49), the matter density parameter in Eq. (43) can be expressed as

$$w_m(z) = w_{m,0}(1+z)^{1-2q_0}(1+z^2)^{-q_1}. \tag{53}$$

Figure 1b shows the changes in the matter and non-metricity density parameters based on the specified values of the model parameters q_0 and q_1 from Ref. [124]. The plots reveal that the matter density parameter reaches the value of 1 between redshift $1 \lesssim z \lesssim 2$ for the H(z), SNIa, and H(z) + SNIa datasets, but for the H(z) + SNIa + BAO/CMB datasets, it does not happen. Based on the analysis of the f(Q) gravity found in Eq. (51), it is not surprising that the parameterization (49) does not result in a standard CDM that aligns with the thermal history.

Based on the parameters q_0 and q_1 provided in [124], the redshift z of transition can be found by setting $\omega^{\rm Tot}(z) = -1/3$. This results in $z \backsimeq 0.71$, 0.72, 0.8, and 0.54 in the H(z), SNIa, H(z) + SNIa, and H(z) + SNIa + BAO/CMB datasets, respectively. The depicted evolution of $\omega^{Tot}(z)$ can be seen in Fig. 1c. While the graphs display the transition redshift in line with observations, they do not align with the standard CDM behavior (i.e., $\omega^{\rm Tot}(z) = 0$) at high redshifts. This confirms the inefficiency of the model at the earlier phases (large redshifts). We also assess the symmetric teleparallel EoS parameter linked to the parametric expres-

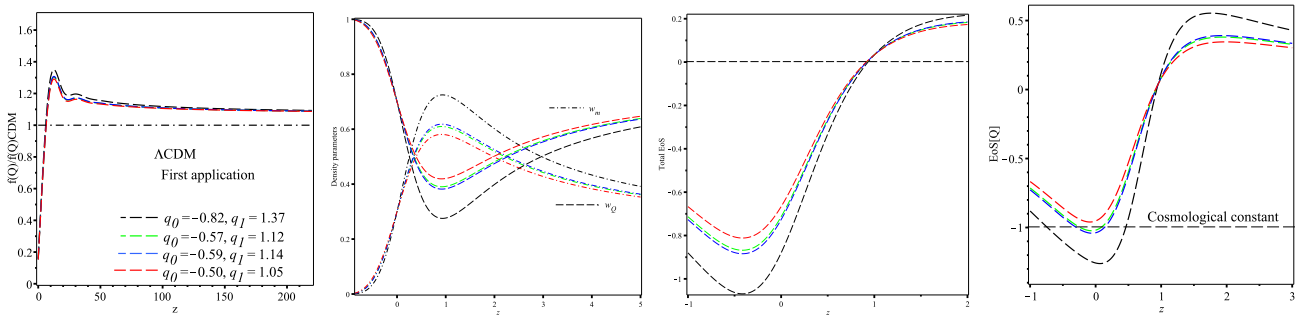

(a) $f(Q)$ gravity (b) w_m, w_Q evolution (c) ω^{Tot} evolution (d) ω_Q evolution

Fig. 2 The best-fit values of model 1 parameters (q_0, q_1) are taken according to the constraint (55). The model parameter q_0 is kept fixed to its value as measured in [124], since it is compatible with the present values of other cosmological parameters. However, the model parameter q_1 is recalculated to fulfill (55) as given on the plots. **a** The behavior of f(Q) gravity, which matches ΛCDM at large redshifts in contrast to the corresponding plots in Fig. 1a. **b** The matter density parameter no longer crosses the unit boundary line, and consequently the non-metricity density parameter does not have negative values. **c** The total EoS shows that the universe can effectively produce a standard CDM-dominant era at large redshifts as $\omega^{Tot} \to 0$. **d** The non-metricity EoS has finite values at all redshifts. The numerical values of q_0 and q_1 presented in panel **a** of this figure are also used in panels **b–d**

sion (49)

$$\omega_{\rm Q}(\rm z) = \frac{2(1+\rm z)^{2q_0}\left[(q_0-\frac{1}{2})+\frac{q_1 z(1+z)}{1+z^2}\right]}{3\left[(1+\rm z)^{2q_0}-\frac{w_{0,m}(1+z)}{(1+z^2)^{q_1}}\right]}. \tag{54}$$

Based on the parameters q_0 and q_1 presented in [124], we illustrate the variation of $\omega_{\rm Q}(z)$ in Fig. 1d, which indicates that the symmetric teleparallel EoS parameter changes in a phantom-like manner at low redshifts. A potential phase transition is observed at redshifts $z \sim 1.19$, $z \sim 1.87$, $z \sim 1.47$, and $z \sim 10.29$ in the H(z), SNIa, H(z) + SNIa, and H(z) + SNIa + BAO/CMB datasets as ω_Q approaches positive or negative infinity. Additionally, the model predicts that it will cross the phantom divide line in the future and enter a quintessence-like state. Surprisingly, the phase changes in symmetric teleparallel gravity are linked to the point where the matter density parameter, $w_m(z)$, crosses the unit boundary line (or when w_Q enters the negative region), as illustrated in Fig. 1b and d.

In the rest of this application, we demonstrate how the model parameters can be constrained in order to achieve feasible cosmic development. If the predicted model parameter values match their measured values, then the assumed parameterization may accurately depict cosmic history. In fact, we require the matter density parameter to approach a maximum value of $w_m(z) = 1$ as z approaches infinity. This requirement is helpful in imposing an additional limitation on the independent variables q_0 and q_1. To expand further, we express the matter density parameter (53) asymptotically up to the second order of the redshift as

$$\widetilde{w}_m(z) \approx w_{m,0}\left(\frac{1}{z}\right)^{2(q_0+q_1)}(1+z-2q_0)+O(1/z^2).$$

In order for the models to be feasible, $\widetilde{w}_m(z)$ must be less than or equal to 1; otherwise, the symmetric teleparallel density parameter would need to decrease to negative values. This restricts q_1 to a lower limit:

$$q_1 \geq \lim_{z\to\infty}\frac{\ln\left[z^{-2q_0}(1+z-2q_0)w_{0,m}\right]}{\ln z^2} = \frac{1}{2}-q_0. \tag{55}$$

Equation (55) limits the selection of model parameters to

$$q_0+q_1 \geq 0.5. \tag{56}$$

When $q_0+q_1 < 0.5$, the density parameter of matter would surpass 1 at a certain redshift in the past. The closer that $q_0+q_1 \geq 0.5 \to 0.5^-$, the closer the previous $w_m(z)$ crossing occurs to the unit boundary, specifically at a higher z value. This is evident in Fig. 1b, with the totals of q_0+q_1 being 0.16, 0.13, and 0.08 for the H(z), SNIa, and H(z) + SNIa datasets. The sum of q_0+q_1 for the combination H(z) + SNIa + BAO/CMB equals 0.28, nearing the critical value of 0.5. Thus, the matter density parameter crosses the unit boundary at a higher redshift around $z \sim 10$. Nevertheless, these patterns do not align with the expected ΛCDM behavior, as stated previously.

To improve the model forecasts, we set the q_0 value taken from [124], as it aligns with the current values of other cosmological parameters. Nonetheless, we employ the matter domination condition (55) to recompute the respective q_1 value for every set of data. In this instance, we improve the development of f(Q) gravity, as depicted in Fig. 2a. When comparing with Fig. 1a, we observe that the graphs are in agreement with the ΛCDM model at high redshifts. Alternatively, the universe can be effectively characterized by a standard CDM matter domination era with $\omega^{\rm Tot} \to 0$ at high redshifts, as shown in Fig. 2c. The matter density parameter

Table 1 The first application's primary outcomes are determined by the values of (q_0, q_1) parameters presented in [124] and the matter density parameter restriction (55). Later on, we maintain the stringently measured values of q_0 but adjust the values of q_1 as needed to meet the constraint

Dataset	q_0	q_1	f(Q)/ΛCDM compatibility	$w_m(z) \leq 1$ constraint	Non-metricity EoS, w_Q	Viability
H(z)	−0.82	0.98	Not	Violated ($z \sim 1.31$)	Diverges[a]($z \sim 1.31$)	Not
SNIa	−0.57	0.70	Not	Violated ($z \sim 1.29$)	Diverges[a] ($z \sim 1.29$)	Not
H(z) + SNIa	−0.59	0.67	Not	Violated ($z \sim 1.5$)	Diverges[a] ($z \sim 1.5$)	Not
H(z) + SNIa + BAO/CMB	−0.50	0.78	Not	Violated ($z \sim 0.82$)	Finite ($z \sim 0.82$)	Not
Using constraint (55)						
H(z)	−0.82	1.37	Approximately	Fulfilled	Finite	*Not*[b]
SNIa	−0.57	1.12	Approximately	Fulfilled	Finite	Not[b]
H(z) + SNIa	−0.59	1.14	Approximately	Fulfilled	Finite	Not[b]
H(z) + SNIa + BAO/CMB	−0.50	1.05	Approximately	Fulfilled	Finite	Not[b]

[a]Note that the non-metricity EoS diverges when the matter density parameter exceeds the unit boundary line (equivalently, when the torsion density parameter becomes negative); see Fig. 1b and d

[b]Although the enhanced parameters—using the matter density parameter constraint (55)—give f(Q) gravity with better compatibility with ΛCDM and smooth ω_T, it cannot produce viable patterns of the matter density parameter, as seen in Fig. 2b

remains below the unit boundary line, yet it displays behavior that does not align with the matter domination era, as is clear from Fig. 2b. Lastly, it is worth mentioning that with the improved version, the symmetric teleparallel EoS no longer shows any phase transitions, and ω_Q is now a finite value at all redshifts, as shown in Fig. 2d. Table 1 provides an overview of the outcomes of the first application based on the model parameters q_0 and q_1 specified in Ref. [124] and utilizing the matter density constraint (55).

6.3 Second application

In this application, we investigate an alternative parameterization q(z) as follows [97]:

$$X(z) = \frac{\ln(\alpha + z)}{(1+z)} - \ln\alpha, \quad \alpha > 1. \tag{57}$$

Utilizing the parameterization mentioned above, the deceleration parameter (48) was tested against observational datasets, namely JLA SNIa and BAO/CMB. The optimal values for the independent parameters q_0 and q_1 were determined within 1σ uncertainty [97]. Various values of the parameter α have been demonstrated, including ($\alpha = 2$, $q_0 = -0.45$, $q_1 = -2.56$), ($\alpha = 3$, $q_0 = -0.54$, $q_1 = -1.35$), ($\alpha = 4$, $q_0 = -0.56$, $q_1 = -1.03$), and ($\alpha = 5, q_0 = -0.56, q_1 = -0.85$). Furthermore, it has been demonstrated that at the current epoch $z = 0$, the described parameterizations result in the deceleration parameter being equal to a value of $q = q_0$, whereas at high redshifts, one can achieve the matter-dominated era, $q = \frac{1}{2}$, through the constraint $q_1 = \frac{2q_0 - 1}{2\ln\alpha}$. By using the parametric form given by Eqs. (57) and (31), the Hubble–redshift relation can be expressed.

$$H(z) = H_0 \alpha^{\xi} (1+z)^{\beta} (\alpha + z)^{-\frac{(\alpha+z)\xi}{(1+z)\alpha}}, \tag{58}$$

with ξ being determined by $\frac{q_1\alpha}{\alpha - 1}$ and β calculated as $1 + q_0 + \frac{\xi}{\alpha} - q_1 \ln\alpha$. Moreover, through the utilization of Eq. (37), we derive the form of f(z) that governs the gravity sector as

$$f(z) = -6\Omega_{m,0}H_0^2 \frac{(1+z)^{\beta}}{(\alpha+z)^{\frac{(\alpha+z)\xi}{(1+z)\alpha}}} \int_0^z \frac{(1+\tilde{z})^{2-\beta}\left(1 + q_0 + q_1\frac{\ln(\alpha+\tilde{z})}{(1+\tilde{z})} - \ln\alpha\right)}{(\alpha+\tilde{z})^{-\frac{(\alpha+\tilde{z})\xi}{(1+\tilde{z})\alpha}}} d\tilde{z}. \tag{59}$$

In Fig. 3a, we plot the f(Q) gravity found in [97] against the redshift for various measurements of q_0 and q_1. Just like the first application, the charts demonstrate significant differences between the theory and the ΛCDM cosmology, which is not commonly preferred. This must be evident in changing cosmological parameters such as the matter density parameter.

Next, we analyze the total EoS parameter using the parameterization given by Eq. (57). Here, Eq. (29) is formulated in terms of z for the second application as

$$\omega^{\text{Tot}}(z) = -\frac{1}{3} + \frac{2}{3}\left[q_0 + q_1\left(\frac{\ln(\alpha+z)}{(1+z)} - \ln\alpha\right)\right]. \tag{60}$$

The transition redshift z can be found by setting $\omega^{\text{Tot}}(z) = -1/3$, using the values of q_0 and q_1 provided in [97]. According to the SNIa + BAO/CMB datasets, the transition redshift is approximately 1.32, 0.98, 0.88, and 0.86 for different values of α ranging from 2 to 5. By utilizing

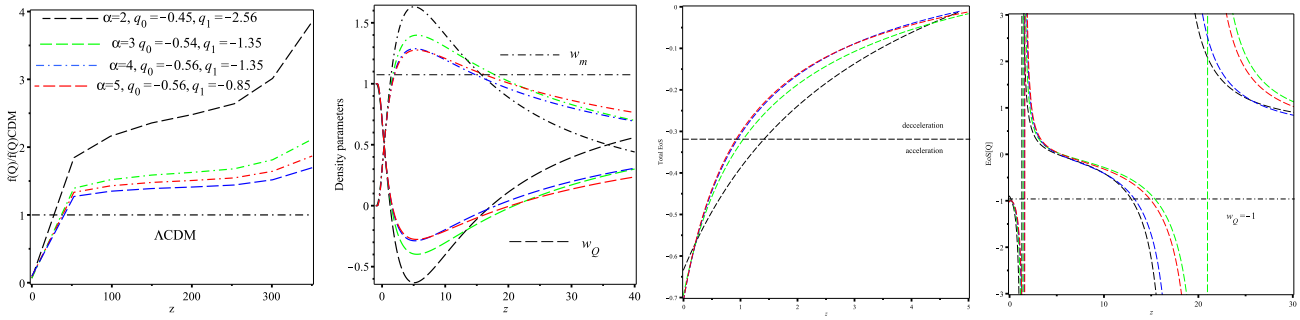

(a) f(Q) behavior (b) $w_m(z)$, $w_Q(z)$ behavior (c) ω^{Tot} behavior (d) ω_Q behavior

Fig. 3 **a** The behavior of f(Q(z)) gravity normalized to ΛCDM. **b** Matter density parameter. **c** The total EoS. **d** The EoS for symmetric teleparallel dark energy. All the numerical values of q_0 and q_1 presented in panel **a** are used in panels **b–d**

Eq. (57), Eq. (43) can be expressed as

$$w_m(z) = \frac{w_{m,0}}{\alpha^{2\xi}}(1+z)^{3-2\beta}(\alpha+z)^{2\frac{(\alpha+z)\xi}{(1+z)\alpha}}. \tag{61}$$

Figure 3b shows how the matter and symmetric teleparallel density parameters evolve based on the calculated values of the model parameters q_0 and q_1 from Ref. [97]. The graphs demonstrate that the matter density parameter $w_m(z)$ is between 0 and 1 at high redshifts, reaching a maximum at low redshifts and intersecting the unit boundary line at redshifts approximately 15.6, 16.2, 18.2, and 18.8 for values of α ranging from 2 to 5. However, the density decreases again as it crosses the unit boundary line at redshifts $z \sim 0.99$, 1.18, 1.28 and 1.3 for values of $\alpha = 2\cdots5$. According to the evaluation of the derived f(Q) gravity, as shown in Eq. (59), the parameterizations (57) do not give rise to a period dominated by matter that aligns with the thermal history.

The plot in Fig. 3c shows the variation of $\omega^{Tot}(z)$ over time. Despite the plots displaying transition redshift in line with observations, they do not align with the standard CDM behavior ($\omega^{Tot}(z) = 0$) at high redshift. This reaffirms the lack of effectiveness of the model during the initial stages, i.e., at high redshifts.

Additionally, we assess the symmetric teleparallel parameter linked to the parametric expression (57) as

$$\omega_Q(z) = \frac{-1+2q_0+2q_1\left[\frac{\ln(\alpha+z)}{1+z}-\ln\alpha\right]}{3-3w_{m,0}\alpha^{\xi}(1+z)^{3-2s}(\alpha+z)^{\frac{2\xi(\alpha+z)}{\alpha(1+z)}}}. \tag{62}$$

Based on the parameters q_0 and q_1 described in [97], we illustrate the behavior of $\omega_Q(z)$ in Fig. 3d, which shows that the symmetric teleparallel EoS parameter transitions to a phantom-like state at lower redshifts. We observe a rapid change in phase at redshifts of approximately $z = 15.78$, 17.96, 14.89, and 16.41 for the parameters α ranging from 2 to 5 when ω_Q approaches infinity in opposite directions. Additionally, another phase change can occur at lower redshifts $z \sim 1.03$, 1.2, 1.3, and 1.33 for the parameters $\alpha = 2\cdots5$, respectively. The model predicts a gradual transition across the phantom divide line towards a quintessence-like state in the future. Notably, the phase changes in symmetric teleparallel theory are linked to crossing the matter density parameter, $w_m(z)$, at the unit boundary line, as depicted in Fig. 3b and d.

Next, we demonstrate how the model parameter can be constrained to generate feasible cosmic development. If the model's predicted parameter values match the measured values, then the chosen parameterizations can accurately describe the history of the universe. In reality, it is necessary for the matter density parameter to approach a maximum value $w_m(z) = 1$ as z approaches infinity. This requirement is beneficial for imposing an additional restriction on the independent variables q_0 and q_1. To further elaborate, we express the asymptotic series of the matter density parameter (61) up to the second order of the redshift and obtain

$$\widetilde{w}_m(z) \approx \frac{w_{m,0}}{\alpha^{2\xi}} z^{1-2q_0+2q_1\ln\alpha}.$$

In order for the models to be feasible, $\widetilde{w}_m(z)$ must be less than or equal to 1; otherwise, the symmetric teleparallel density parameter would need to decrease to negative values. This restricts q_1 to a lower limit as follows:

$$q_1 \le \lim_{z\to\infty} -\frac{1}{2}\frac{\left(\ln\frac{1}{w_{m,0}z}+2q_0\ln z\right)(\alpha-1)}{\left(\alpha-\ln\frac{1}{z}+\alpha\ln\frac{1}{z}\right)\ln\alpha} = \frac{2q_0-1}{2\ln\alpha}. \tag{63}$$

The constraints ensure that the parameterization (57) is able to approach $q \to 1/2$ as $z \to \infty$, as discussed in [97]. In reality, however, this will not stop the density parameter from crossing the unit boundary at lower redshifts; it simply smooths out the peaks across a broad range of redshifts. In this case, it may be more important to regulate the amplitude of the $w_m(z)$ peak so that it does not exceed the unit boundary. To ensure the feasibility of this model at least for

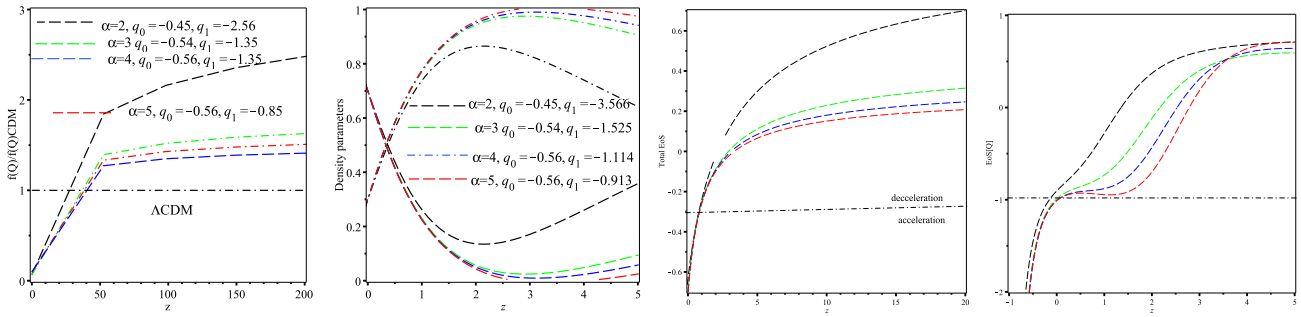

(a) f(Q) theory (b) w_m, w_Q behavior (c) ω^{Tot} behavior (d) ω_Q behavior

Fig. 4 The values of second application parameters (q_0, q_1) were determined based on the constraint (64) for the best fit. The value of the model parameter q_0 remains unchanged from the measurement in [97], as it aligns with the current values of other cosmological parameters. Nevertheless, the parameter q_1 is adjusted in order to satisfy Eq. (64), as shown in the graphs. **a** The f(Q) theory matches ΛCDM at large redshifts in contrast to the corresponding plots in Fig. 3a. **b** The density parameter of matter no longer exceeds the unit boundary line, leading to the symmetric teleparallel density parameter having no negative values. **c** The total EoS demonstrates that at high redshifts, the universe can effectively generate a dominant standard CDM era as $\omega^{Tot} \to 0$. **d** The dark energy EoS symmetric teleparallel has values that are finite at every redshift. The numerical values of q_0 and q_1 presented in panel **b** are used in panels **c–d**

Table 2 The primary outcomes of the second application based on the values of (q_0, q_1) parameters presented in [97] and utilizing the matter density parameter constraint (64). In the upcoming case, we maintain the precise measured values q_0 unchanged, but adjust the values of q_1 to satisfy the requirement

Dataset	α	q_0	q_1	f(Q)/ΛCDM compatibility	$w_m(z) \leq 1$ constraint	Non-metricity EoS, w_Q	Viability
JLA SNIa + BAO/CMB	2	−0.45	−2.56	Not	Violated	Diverges[a]	Not
JLA SNIa + BAO/CMB	3	−0.54	−1.35	Not	Violated	Diverges[a]	Not
JLA SNIa + BAO/CMB	4	−0.56	−1.03	Not	Violated	Diverges[a]	Not
JLA SNIa + BAO/CMB	5	−0.56	−0.85	Not	Violated	Diverges[a]	Not
Utilizing limitation (64)							
JLA SNIa + BAO/CMB	2	−0.45	−3.366	Not	Fulfilled	Does not diverge	Not[b]
JLA SNIa + BAO/CMB	3	−0.54	−1.525	Not	Fulfilled	Does not diverge	Not[b]
JLA SNIa + BAO/CMB	4	−0.56	−1.114	Not	Fulfilled	Does not diverge	Not[b]
JLA SNIa + BAO/CMB	5	−0.56	−0.913	Not	Fulfilled	Does not diverge	Not[b]

[a]The symmetric teleparallel EoS experiences two divergences when the density parameter of matter crosses the unit boundary line twice, as depicted in Fig. 3b and d

[b]While the density parameter matter constraint (64) results in smooth w_Q patterns (Fig. 4d), it fails to generate f(Q) gravity that is more compatible with ΛCDM, as indicated in Fig. 4a

low redshifts z, we impose the condition $w_m(z) = 1$ *for low values of redshifts*. By utilizing Eq. (61), we can determine q_1 by solving this constraint.

$$q_1 = \frac{(\alpha-1)(1+z_{lower})\left[\ln(1+z_{lower})^{2q_0-1} - \ln w_{m,0}\right]}{\ln\left[\frac{(1+z_l)^{2[(\alpha-1)\ln\alpha-1](1+z_l)}(\alpha+z_{lower})^{2(\alpha+z_{lower})}}{\alpha^{2\alpha(1+z_{lower})}}\right]}. \tag{64}$$

It is justifiable to maintain q_0 as determined in [97] when the $a_m(z_{lower})$ peak occurs at $z_{lower} = 3$, resulting in q_1 approximately equal to −3.366, −1.525, −1.114, and −0.913 for α values ranging from $2 \to 5$, respectively. In this instance, we plot the progression of f(Q) gravity, specifically (59), as depicted in Fig. 4a. In comparison to Fig. 3a, we observe that the plots continue to disagree with the ΛCDM model at high redshifts. The matter density parameter remains below the unit boundary line, but its behavior remains incongruent with the matter domination era which is clearly shown in Fig. 4b. Conversely, the universe is unable to accurately depict the standard CDM matter domination era because omega$^{Tot} > 0$ is observed at high redshifts, as shown in Fig. 4c. It is important to mention that the improved symmetric teleparallel equation of state no longer shows any signs of phase transitions, while ω_Q now remains finite at all levels of redshift, as depicted in Fig. 4d. Table 2 presents a summary of the outcomes of the second application based on the specified values of the model parameters q_0 and q_1 presented in [97], incorporating the matter density restriction (64).

6.4 Third application

Now we will rebuild the theory of f(Q) gravity based on the parametric representation of the effective equation of state previously used in Ref. [117],

$$\omega^{Tot} = -\frac{1}{1+\alpha_1(1+z)^{\alpha_2}}, \tag{65}$$

where the two parameters of the model are denoted by α_1 and α_2. At high redshifts, the universe essentially creates standard CDM as ω^{Tot} approaches zero. As z approaches -1, the universe essentially moves towards the de Sitter phase when ω^{Tot} approaches -1. This is clearly illustrated in Fig. 5a. Essentially, this design has the potential to create a thriving cosmic timeline. Utilizing (29), we can express the deceleration parameter related to the abovementioned parameterization as

$$\mathrm{q(z)} = -1 + \frac{3\alpha_1(1+\mathrm{z})^{\alpha_2}}{2\left[1+\alpha_1(1+\mathrm{z})^{\alpha_2}\right]}. \tag{66}$$

Plugging the above data into Eq. (31), the Hubble parameter is determined as

$$\mathrm{H(z)} = \mathrm{H_0}\left[\frac{1+\alpha_1(1+\mathrm{z})^{\alpha_2}}{1+\alpha_1}\right]^{\frac{3}{2\alpha_2}}. \tag{67}$$

It is evident that when $\alpha_2 = 3$, the model results in the ΛCDM model. In this case, we find that $w_{m,0} = \frac{\alpha_1}{1+\alpha_1}$, which is also expressed as $\alpha_1 = \frac{w_{m,0}}{1-w_{m,0}}$. The value $w_{m,0} = 0.297$ is adopted from the measurement in Ref. [117]. In dynamic DE models that are feasible, it is likely that the value of α_2 will be around 3. Alternatively, we employ Eq. (38) to calculate f(Q) gravity, leading to the parametric expression (65)

$$f(z) = -9\alpha_1\Omega_{m,0}H_0^2\left[1+\alpha_1(1+z)^{\alpha_2}\right]^{\frac{3}{2\alpha_2}} \times \int_0^z \frac{(1+\tilde{z})^{\alpha_2+2}}{\left[1+\alpha_1(1+\tilde{z})^{\alpha_2}\right]^{1+\frac{3}{2\alpha_2}}} d\tilde{z}.$$

In Fig. 5b, we plot the evolution of the f(Q) gravity under consideration versus ΛCDM for different values of the model parameters α_1 and α_2 according to the dataset used [117]. The plots show systematic deviation of the f(Q) theory from ΛCDM when the dataset combination SN + observed Hubble data (OHD) is used, since it does not oscillate about ΛCDM. Otherwise, the theory is compatible with ΛCDM. The reasons for these results will be explained later within this application.

Using the deceleration (66), the matter density parameter (43) reads

$$w_m(z) = w_{m,0}\,(1+z)^3\left[\frac{1+\alpha_1}{1+\alpha_1(1+z)^{\alpha_2}}\right]^{\frac{3}{\alpha_2}}. \tag{68}$$

In Fig. 5c, we plot the evolution of the matter density parameter using different values of the model parameters. As seen, the density matter exceeds the unity at redshift $z \sim 2$ when the parameters are fitted with the dataset SN + OHD. On the other hand, the density matter has a slight but not trivial deviation form ΛCDM at large z when the parameters are fitted with the dataset $H(z)+SN$. However, it evolves very similar to ΛCDM when the BAO and CMB (shift parameters) are added. In fact, these results are in agreement with the plots of Fig. 5b.

Substituting from (67) and (68) in (39), we evaluate the symmetric teleparallel (DE) EoS as

$$w_Q = -\frac{\left[1+\alpha_1(1+z)^{\alpha_2}\right]^{\frac{3}{\alpha_2}} - \alpha_1(1+z)^{\alpha_2}\left[1+\alpha_1(1+z)^{\alpha_2}\right]^{\frac{3}{\alpha_2}-1}}{\left[1+\alpha_1(1+z)^{\alpha_2}\right]^{\frac{3}{\alpha_2}} - w_{m,0}(1+z)^3(1+\alpha_1)^{\frac{3}{\alpha_2}}}. \tag{69}$$

As seen from Fig. 5d, the symmetric teleparallel EoS diverges at redshift $z \sim 2$ when the SN + OHD + BAO dataset is used. We note that the symmetric teleparallel phase transition is associated with the crossing of the unit boundary line by the matter density parameter, as seen in Fig. 5c.

In order to constrain the model parameters, we follow the treatment of Sect. 6.1 by requiring the matter density parameter (68) to reach a maximal value $\Omega_{m,0} = 1$ asymptotically, i.e., as $z \to \infty$. This condition is useful for putting a lower bound on the parameter α. Specifically, we write the leading term of the asymptotic expansion of the matter density parameter

$$\widetilde{w}_m(z) \approx w_{m,0}\left(1+\frac{1}{\alpha_1}\right)^{\frac{3}{\alpha_2}}.$$

For viable models, we need $\widetilde{w}_m(z) \leq 1$; otherwise, the symmetric teleparallel density parameter would drop below zero. This constrains α_1 to a minimum value

$$\alpha_{1\,min} = \frac{w_{m,0}^{\frac{\alpha_2}{3}}}{1-w_{m,0}^{\frac{\alpha_2}{3}}}. \tag{70}$$

If α_1 goes below the above minimum, the matter density parameter would exceed unity at some past redshift, and the torsion density parameter would subsequently become negative. For example, the measured value of the parameter $\alpha_1 = 0.445$ according to the dataset SN + OHD [117] is less than the allowed minimum value $\alpha_{1\,min} = 0.4728$ according to the density matter constraint[2] (70). Therefore, we understand the incompatibility of the model results (see Fig. 5c) whenever the SN + OHD dataset is used. On the contrary, we find that the measured values $\alpha_1 = 0.409 > \alpha_{1\,min} = 0.3904$

[2] Note that we take $w_{m,0} = 0.297$ as derived in [117] and $\alpha_2 = 2.8$ as measured using the SN + OHD dataset.

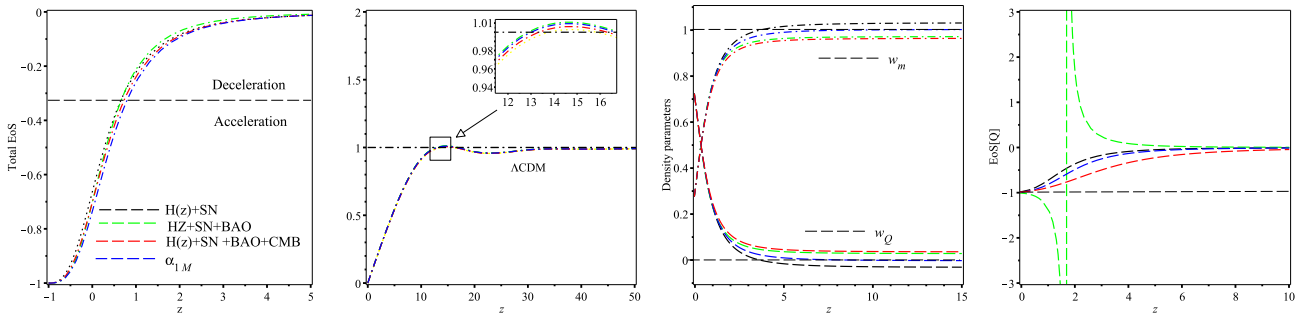

(a) ω^{Tot} according to [117] (b) ω^{Tot} according to [117] (c) $w_m(z)$, $w_Q(z)$ according to [117] (d) ω_Q according to [117]

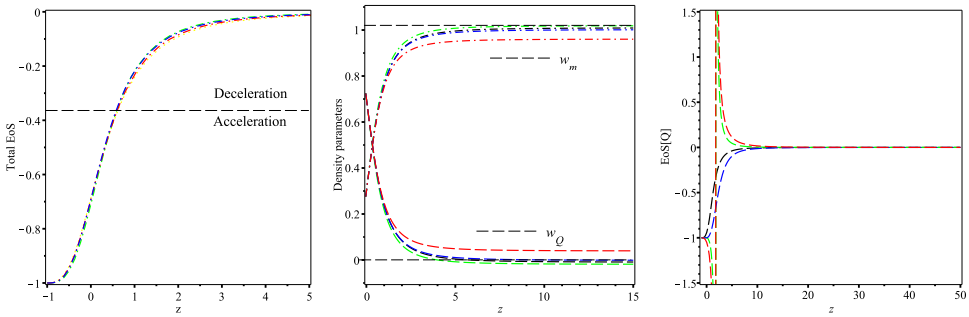

(e) ω^{Tot} using the constraint (70) (f) w_m, w_Q using the constraint (70) (g) w_Q using the constraint (70)

Fig. 5 In sub-figures **a**–**d**, the best-fit values of the model parameters (α_1, α_2) are taken according to the dataset combination as measured in [117]; (0.445, 2.8) for SN + OHD, (0.409, 3.13) for SN + OHD + BAO, (0.444, 2.907) for SN + OHD + BAO + CMB, and ($\alpha = \frac{\Omega_{m,0}}{1-\Omega_{m,0}}$, $\alpha_2 = 3$) for ΛCDM with Planck parameters. In sub-figures e-g, we use the constraint (70) to determine α_{min} for different choices of α_2, while the additive constant is taken as $\delta\alpha_1 = 10^{-3}$. The labels used in sub-figure **a** are the same as in **b**–**g**

Table 3 The main results of model 3 according to the values of $(\alpha_1,\ \alpha_2)$ parameters as given in Ref. [117] and by using the matter density parameter constraint (70), where $\alpha_1 = \alpha_{1\,min} + \delta\alpha_1 (= 10^{-3})$. In all treatments, we take $\Omega_{m,0} = 0.297$ as derived in [117]

Dataset	α_1	α_2	$f(Q)/\Lambda$CDM compatibility	$w_m(z) \leq 1$ constraint	symmetric teleparallel EoS, w_Q	Viability
SN + OHD	0.445[a]	2.8	Not	Violated	Diverges	Not
SN + OHD + BAO	0.409	3.13	Semi	Fulfilled	Does not diverge	Yes
SN + OHD + BAO+CMB	0.444	2.907	Semi	Fulfilled	Does not diverge	Yes
Using constraint (70)						
Case (i)	0.503	$2.7 \lesssim 3$	Semi	Fulfilled	Does not diverge (quintessence)	Yes
Case (ii)	0.356	$3.3 \gtrsim 3$	Semi	Fulfilled	Does not diverge (quintom)	Yes
Case (iii)	0.421	3	Semi	Fulfilled	Does not diverge (quintessence)	Yes
ΛCDM	$\alpha_{1\,min}$	3	Yes	Fulfilled	-1	Yes

[a]Note that this dataset provides $\alpha_1 < \alpha_{1\,min}$, which explains the violation of the matter density constraint

(using the SN + OHD + BAO dataset) and $\alpha_1 = 0.444 > \alpha_{1\,min} = 0.4438$ (using the SN + OHD + BAO dataset) are compatible and give viable cosmic scenarios.

Notably, for the ΛCDM case ($\alpha_2 = 3$), the minimum value $\alpha_{1\,min} = \frac{w_{m,0}}{w_{\lambda,0}}$ represents the ratio between the matter and the symmetric teleparallel density parameters at present. In Fig. 5e–g, we plot ΛCDM as $n = 3$ and $\alpha_1 = \alpha_{1\,min}$. At those values, we obtain a fixed symmetric teleparallel EoS $w_Q = -1$. If α_1 slightly exceeds $\alpha_{1\,min}$, we list three possible viable cases: (i) For $\alpha_2 \lesssim 3$, we find that w_Q evolves in quintessence with $w_Q \gtrsim -1$ at present. (ii) For $n \gtrsim 3$, the symmetric teleparallel EoS has a quintom behavior, since w_Q crosses the phantom divide line at $z \sim 4$ from quintessence to phantom with $w_Q \lesssim -1$ at present. (iii) For $\alpha_2 = 3$, the symmetric teleparallel EoS evolves in a quintessence regime with $w_Q \sim -1$ at present. In all cases, $w_Q \to 0$ at large

redshifts, which explains the late accelerating expansion, and evolves towards a cosmological constant (pure de Sitter) in the future. We summarize the model results in Table 3.

In conclusion, we find that the effective EoS parameterization (65) produces a viable f(Q) gravity model. However, the model parameters α_2 and α_1 can be better constrained by the upcoming DE surveys to precisely determine the nature of the DE. On the other hand, the f(Q) theory presented in this subsection is capable of producing a dynamical torsional DE; then—in principal—it could be useful to reconcile the local measurement of the Hubble constant with its global measured value.

7 Concluding remarks

Recent discussions have focused on using parametric forms of the deceleration parameter to explain the late accelerating expansion of the universe through a kinematic approach. While certain parametric shapes may help represent the shift from deceleration to acceleration, it is important to analyze them within a dynamic setting or altered gravitational theory. This enables the testing of additional cosmological parameters in the background as well as at the perturbation level of the theory. In this study, we have developed a reconstruction technique for $f(Q)$ gravity that produces any specific q(z) parameterization. We accomplish this through the consistency between the deceleration parameter (31) and f(Q) gravity (33). Moreover, we have obtained two additional reconstruction equations based on the knowledge of either the effective EoS $\omega^{\rm Tot}(z)$ or the DE EoS $\omega_{\rm DE}(z)$.

In this study we have tested three different applications. In the first application, the q(z) parameterization given by Eq. (49) was utilized. We contrast f(Q) gravity with the ΛCDM model and demonstrate the impracticality of the model, even when increasing its parameters. In the second application, we also use the parameterization $q(z)$ given by Eq. (57). Like the first application, it is unable to generate a feasible cosmological situation consistent with ΛCDM. The $\omega^{Tot}(z)$ parameterization (65) was utilized in the third application. The f(Q) gravity model is in good agreement with both ΛCDM predictions and present observational data. We expect the f(Q) gravity to elucidate the properties of dark energy beyond the ΛCDM due to the flexibility of the model to generate a dynamic DE model with quintessence or quintom behavior. In these three applications, the symmetric teleparallel equation of state will diverge if the matter density parameter exceeds the unit boundary line (or if the teleparallel symmetric density parameter becomes negative). The upcoming DE surveys can confirm this feature.

In conclusion, f(Q) modified gravity provides a promising framework within the analysis of the technique for reconstructing the underlying theories that enriches our understanding of cosmic acceleration, offering new avenues for addressing some of the long-standing challenges in cosmology. Nevertheless, a more captivating investigation involves exploring the theory at the perturbation level as well. We will save this task for a later time.

Data Availability Statement This manuscript has no associated data. [Author's' comment: Data sharing not applicable to this article as no datasets were generated or analysed during the current study.]

Code Availability Statement This manuscript has no associated code/software. [Author's comment: Code/Software sharing not applicable to this article as no code/software was generated or analysed during the current study.]

Funded by SCOAP[3].

References

1. R. Penrose, Phys. Rev. Lett. **14**, 57 (1965). https://doi.org/10.1103/PhysRevLett.14.57
2. S. Hawking, Proc. R. Soc. Lond. A **294**, 511 (1966). https://doi.org/10.1098/rspa.1966.0221
3. S. Hawking, Proc. R. Soc. Lond. A **295**, 490 (1966). https://doi.org/10.1098/rspa.1966.0255
4. S. Hawking, Proc. R. Soc. Lond. A **300**, 187 (1967). https://doi.org/10.1098/rspa.1967.0164
5. S.W. Hawking, D.W. Sciama, Comments Astrophys. Space Phys. **1**, 1 (1969)
6. S.W. Hawking, R. Penrose, Proc. R. Soc. Lond. A **314**, 529 (1970). https://doi.org/10.1098/rspa.1970.0021
7. A.G. Riess et al. (Supernova Search Team), Astron. J. **116**, 1009 (1998). https://doi.org/10.1086/300499. arXiv:astro-ph/9805201
8. S. Perlmutter et al. (Supernova Cosmology Project), Astrophys. J. **517**, 565 (1999). https://doi.org/10.1086/307221. arXiv:astro-ph/9812133
9. A. De Felice, S. Tsujikawa, Living Rev. Relativ. **13**, 3 (2010). https://doi.org/10.12942/lrr-2010-3. arXiv:1002.4928 [gr-qc]
10. R. Ferraro, F. Fiorini, Phys. Rev. D **75**, 084031 (2007). https://doi.org/10.1103/PhysRevD.75.084031. arXiv:gr-qc/0610067
11. S. Bahamonde, K.F. Dialektopoulos, C. Escamilla-Rivera, G. Farrugia, V. Gakis, M. Hendry, M. Hohmann, J. Levi Said, J. Mifsud, E. Di Valentino, Rep. Prog. Phys. **86**, 026901 (2023). https://doi.org/10.1088/1361-6633/ac9cef. arXiv:2106.13793 [gr-qc]
12. W. El Hanafy, G.G.L. Nashed, Phys. Rev. D **100**, 083535 (2019). https://doi.org/10.1103/PhysRevD.100.083535. arXiv:1910.04160 [gr-qc]
13. J.M. Nester, H.-J. Yo, Chin. J. Phys. **37**, 113 (1999). arXiv:gr-qc/9809049

14. J. Beltrán Jiménez, L. Heisenberg, T. Koivisto, Phys. Rev. D **98**, 044048 (2018). https://doi.org/10.1103/PhysRevD.98.044048. arXiv:1710.03116 [gr-qc]
15. Y. Akrami et al. (CANTATA), in *Modified Gravity and Cosmology: An Update by the CANTATA Network*, edited by E.N. Saridakis, R. Lazkoz, V. Salzano, P. Vargas Moniz, S. Capozziello, J. Beltrán Jiménez, M. De Laurentis, G.J. Olmo (Springer, 2021). https://doi.org/10.1007/978-3-030-83715-0. arXiv:2105.12582 [gr-qc]
16. R. Aldrovandi, J.G. Pereira, *Teleparallel Gravity: An Introduction* (Springer, Berlin, 2013). https://doi.org/10.1007/978-94-007-5143-9
17. J. Beltrán Jiménez, L. Heisenberg, T.S. Koivisto, Universe **5**, 173 (2019). https://doi.org/10.3390/universe5070173. arXiv:1903.06830 [hep-th]
18. A.A. Starobinsky, Phys. Lett. B **91**, 99 (1980). https://doi.org/10.1016/0370-2693(80)90670-X
19. S. Capozziello, Int. J. Mod. Phys. D **11**, 483 (2002). https://doi.org/10.1142/S0218271802002025. arXiv:gr-qc/0201033
20. S. Nojiri, S.D. Odintsov, Phys. Lett. B **631**, 1 (2005). https://doi.org/10.1016/j.physletb.2005.10.010. arXiv:hep-th/0508049
21. D. Lovelock, J. Math. Phys. **12**, 498 (1971). https://doi.org/10.1063/1.1665613
22. Y.-F. Cai, S. Capozziello, M. De Laurentis, E.N. Saridakis, Rep. Prog. Phys. **79**, 106901 (2016). https://doi.org/10.1088/0034-4885/79/10/106901. arXiv:1511.07586 [gr-qc]
23. Y.-F. Cai, C. Li, E.N. Saridakis, L. Xue, Phys. Rev. D **97**, 103513 (2018). https://doi.org/10.1103/PhysRevD.97.103513. arXiv:1801.05827 [gr-qc]
24. M. Krssak, R.J. van den Hoogen, J.G. Pereira, C.G. Böhmer, A.A. Coley, Class. Quantum Gravity **36**, 183001 (2019). https://doi.org/10.1088/1361-6382/ab2e1f. arXiv:1810.12932 [gr-qc]
25. G.G.L. Nashed, W. El Hanafy, K. Bamba, JCAP **01**, 058 (2019). https://doi.org/10.1088/1475-7516/2019/01/058. arXiv:1809.02289 [gr-qc]
26. S.-F. Yan, P. Zhang, J.-W. Chen, X.-Z. Zhang, Y.-F. Cai, E.N. Saridakis, Phys. Rev. D **101**, 121301 (2020). https://doi.org/10.1103/PhysRevD.101.121301. arXiv:1909.06388 [astro-ph.CO]
27. Y. Huang, J. Zhang, X. Ren, E.N. Saridakis, Y.-F. Cai, Phys. Rev. D **106**, 064047 (2022). https://doi.org/10.1103/PhysRevD.106.064047. arXiv:2204.06845 [astro-ph.CO]
28. Q. Wang, X. Ren, B. Wang, Y.-F. Cai, W. Luo, E.N. Saridakis, Astrophys. J. **969**, 119 (2024). https://doi.org/10.3847/1538-4357/ad47c0. arXiv:2312.17053 [astro-ph.CO]
29. Y.-M. Hu, Y. Zhao, X. Ren, B. Wang, E.N. Saridakis, Y.-F. Cai, JCAP **07**, 060 (2023). https://doi.org/10.1088/1475-7516/2023/07/060. arXiv:2302.03545 [gr-qc]
30. L. Heisenberg, (2023). arXiv:2309.15958 [gr-qc]
31. W. Khyllep, A. Paliathanasis, J. Dutta, Phys. Rev. D **103**, 103521 (2021). https://doi.org/10.1103/PhysRevD.103.103521. arXiv:2103.08372 [gr-qc]
32. S. Mandal, D. Wang, P.K. Sahoo, Phys. Rev. D **102**, 124029 (2020). https://doi.org/10.1103/PhysRevD.102.124029. arXiv:2011.00420 [gr-qc]
33. B.J. Barros, T. Barreiro, T. Koivisto, N.J. Nunes, Phys. Dark Univ. **30**, 100616 (2020). https://doi.org/10.1016/j.dark.2020.100616. arXiv:2004.07867 [gr-qc]
34. J. Lu, X. Zhao, G. Chee, Eur. Phys. J. C **79**, 530 (2019). https://doi.org/10.1140/epjc/s10052-019-7038-3. arXiv:1906.08920 [gr-qc]
35. A. De, L.T. How, Phys. Rev. D **106**, 048501 (2022). https://doi.org/10.1103/PhysRevD.106.048501. arXiv:2208.05779 [gr-qc]
36. R. Solanki, A. De, S. Mandal, P.K. Sahoo, Phys. Dark Univ. **36**, 101053 (2022). https://doi.org/10.1016/j.dark.2022.101053. arXiv:2201.06521 [gr-qc]
37. A. Lymperis, JCAP **11**, 018 (2022). https://doi.org/10.1088/1475-7516/2022/11/018. arXiv:2207.10997 [gr-qc]
38. F. D'Ambrosio, S.D.B. Fell, L. Heisenberg, S. Kuhn, Phys. Rev. D **105**, 024042 (2022). https://doi.org/10.1103/PhysRevD.105.024042. arXiv:2109.03174 [gr-qc]
39. M. Li, D. Zhao, Phys. Lett. B **827**, 136968 (2022). https://doi.org/10.1016/j.physletb.2022.136968. arXiv:2108.01337 [gr-qc]
40. N. Dimakis, A. Paliathanasis, T. Christodoulakis, Class. Quantum Gravity **38**, 225003 (2021). https://doi.org/10.1088/1361-6382/ac2b09. arXiv:2108.01970 [gr-qc]
41. M. Hohmann, Phys. Rev. D **104**, 124077 (2021). https://doi.org/10.1103/PhysRevD.104.124077. arXiv:2109.01525 [gr-qc]
42. A. Kar, S. Sadhukhan, U. Debnath, Mod. Phys. Lett. A **37**, 2250183 (2022). https://doi.org/10.1142/S0217732322501838. arXiv:2109.10906 [gr-qc]
43. W. Wang, H. Chen, T. Katsuragawa, Phys. Rev. D **105**, 024060 (2022). https://doi.org/10.1103/PhysRevD.105.024060. arXiv:2110.13565 [gr-qc]
44. I. Quiros, Phys. Rev. D **105**, 104060 (2022). https://doi.org/10.1103/PhysRevD.105.104060. arXiv:2111.05490 [gr-qc]
45. S. Mandal, P.K. Sahoo, Phys. Lett. B **823**, 136786 (2021). https://doi.org/10.1016/j.physletb.2021.136786. arXiv:2111.10511 [gr-qc]
46. I.S. Albuquerque, N. Frusciante, Phys. Dark Univ. **35**, 100980 (2022). https://doi.org/10.1016/j.dark.2022.100980. arXiv:2202.04637 [astro-ph.CO]
47. G.G.L. Nashed, W. El Hanafy, Eur. Phys. J. C **82**, 679 (2022). https://doi.org/10.1140/epjc/s10052-022-10634-0. arXiv:2208.13814 [gr-qc]
48. S. Capozziello, R. D'Agostino, Phys. Lett. B **832**, 137229 (2022). https://doi.org/10.1016/j.physletb.2022.137229. arXiv:2204.01015 [gr-qc]
49. S. Capozziello, M. Shokri, Phys. Dark Univ. **37**, 101113 (2022). https://doi.org/10.1016/j.dark.2022.101113. arXiv:2209.06670 [gr-qc]
50. N. Dimakis, M. Roumeliotis, A. Paliathanasis, P.S. Apostolopoulos, T. Christodoulakis, Phys. Rev. D **106**, 123516 (2022). https://doi.org/10.1103/PhysRevD.106.123516. arXiv:2210.10295 [gr-qc]
51. R. D'Agostino, R.C. Nunes, Phys. Rev. D **106**, 124053 (2022). https://doi.org/10.1103/PhysRevD.106.124053. arXiv:2210.11935 [gr-qc]
52. S.A. Narawade, B. Mishra, Ann. Phys. **535**, 2200626 (2023). https://doi.org/10.1002/andp.202200626. arXiv:2211.09701 [gr-qc]
53. E.D. Emtsova, A.N. Petrov, A.V. Toporensky, Eur. Phys. J. C **83**, 366 (2023). https://doi.org/10.1140/epjc/s10052-023-11460-8. arXiv:2212.03755 [gr-qc]
54. S. Bahamonde, G. Trenkler, L.G. Trombetta, M. Yamaguchi, Phys. Rev. D **107**, 104024 (2023). https://doi.org/10.1103/PhysRevD.107.104024. arXiv:2212.08005 [gr-qc]
55. O. Sokoliuk, S. Arora, S. Praharaj, A. Baransky, P.K. Sahoo, Mon. Not. R. Astron. Soc. **522**, 252 (2023). https://doi.org/10.1093/mnras/stad968. arXiv:2303.17341 [astro-ph.CO]
56. A. De, T.-H. Loo, E.N. Saridakis, JCAP **03**, 050 (2024). https://doi.org/10.1088/1475-7516/2024/03/050. arXiv:2308.00652 [gr-qc]
57. N. Dimakis, M. Roumeliotis, A. Paliathanasis, T. Christodoulakis, Eur. Phys. J. C **83**, 794 (2023). https://doi.org/10.1140/epjc/s10052-023-11964-3. arXiv:2304.04419 [gr-qc]
58. S.K. Maurya, A. Errehymy, M.K. Jasim, M. Daoud, N. Al-Harbi, A.-H. Abdel-Aty, Eur. Phys. J. C **83**, 317 (2023). https://doi.org/10.1140/epjc/s10052-023-11447-5
59. J. Ferreira, T. Barreiro, J.P. Mimoso, N.J. Nunes, Phys. Rev. D **108**, 063521 (2023). https://doi.org/10.1103/PhysRevD.108.063521. arXiv:2306.10176 [astro-ph.CO]

60. S. Capozziello, V. De Falco, C. Ferrara, Eur. Phys. J. C **83**, 915 (2023). https://doi.org/10.1140/epjc/s10052-023-12072-y. arXiv:2307.13280 [gr-qc]
61. M. Koussour, A. De, Eur. Phys. J. C **83**, 400 (2023). https://doi.org/10.1140/epjc/s10052-023-11547-2. arXiv:2304.11765 [gr-qc]
62. J.A. Nájera, C.A. Alvarado, C. Escamilla-Rivera, Mon. Not. R. Astron. Soc. **524**, 5280 (2023). https://doi.org/10.1093/mnras/stad2180. arXiv:2304.12601 [gr-qc]
63. L. Atayde, N. Frusciante, Phys. Rev. D **107**, 124048 (2023). https://doi.org/10.1103/PhysRevD.107.124048. arXiv:2306.03015 [astro-ph.CO]
64. A. Paliathanasis, N. Dimakis, T. Christodoulakis, Phys. Dark Univ. **43**, 101410 (2024). https://doi.org/10.1016/j.dark.2023.101410. arXiv:2308.15207 [gr-qc]
65. P. Bhar, Eur. Phys. J. C **83**, 737 (2023). https://doi.org/10.1140/epjc/s10052-023-11865-5
66. A. Mussatayeva, N. Myrzakulov, M. Koussour, Phys. Dark Univ. **42**, 101276 (2023). https://doi.org/10.1016/j.dark.2023.101276. arXiv:2307.00281 [gr-qc]
67. A. Paliathanasis, Phys. Dark Univ. **43**, 101388 (2024). https://doi.org/10.1016/j.dark.2023.101388. arXiv:2309.14669 [gr-qc]
68. S. Mandal, S. Pradhan, P.K. Sahoo, T. Harko, Eur. Phys. J. C **83**, 1141 (2023). https://doi.org/10.1140/epjc/s10052-023-12339-4. arXiv:2310.00030 [gr-qc]
69. A. Pradhan, A. Dixit, M. Zeyauddin, S. Krishnannair, Int. J. Geom. Methods Mod. Phys. **21**, 2450167 (2024). https://doi.org/10.1142/S0219887824501676. arXiv:2310.02267 [gr-qc]
70. S. Capozziello, M. Capriolo, S. Nojiri, Phys. Lett. B **850**, 138510 (2024). https://doi.org/10.1016/j.physletb.2024.138510. arXiv:2401.06424 [gr-qc]
71. P. Bhar, A. Malik, A. Almas, Chin. J. Phys. **88**, 839 (2024). https://doi.org/10.1016/j.cjph.2024.02.016
72. D. Mhamdi, A. Bouali, S. Dahmani, A. Errahmani, T. Ouali, Eur. Phys. J. C **84**, 310 (2024). https://doi.org/10.1140/epjc/s10052-024-12549-4
73. R.-H. Lin, X.-H. Zhai, Phys. Rev. D **103**, 124001 (2021) [note Erratum: Phys. Rev. D 106, 069902 (2022)]. https://doi.org/10.1103/PhysRevD.103.124001. arXiv:2105.01484 [gr-qc]
74. Y. Yang, X. Ren, B. Wang, Y.-F. Cai, E.N. Saridakis, (2024). arXiv:2404.12140 [astro-ph.CO]
75. A. De, S. Mandal, J.T. Beh, T.-H. Loo, P.K. Sahoo, Eur. Phys. J. C **82**, 72 (2022). https://doi.org/10.1140/epjc/s10052-022-10021-9. arXiv:2201.05036 [gr-qc]
76. F.K. Anagnostopoulos, S. Basilakos, E.N. Saridakis, Phys. Lett. B **822**, 136634 (2021). https://doi.org/10.1016/j.physletb.2021.136634. arXiv:2104.15123 [gr-qc]
77. R. Solanki, A. De, P.K. Sahoo, Phys. Dark Univ. **36**, 100996 (2022). https://doi.org/10.1016/j.dark.2022.100996. arXiv:2203.03370 [gr-qc]
78. J.-T. Beh, T.-H. Loo, A. De, Chin. J. Phys. **77**, 1551 (2022). https://doi.org/10.1016/j.cjph.2021.11.026. arXiv:2107.04513 [gr-qc]
79. A. De, T.-H. Loo, Class. Quantum Gravity **40**, 115007 (2023). https://doi.org/10.1088/1361-6382/accef7. arXiv:2212.08304 [gr-qc]
80. J. Beltrán Jiménez, L. Heisenberg, T.S. Koivisto, S. Pekar, Phys. Rev. D **101**, 103507 (2020). https://doi.org/10.1103/PhysRevD.101.103507. arXiv:1906.10027 [gr-qc]
81. N. Frusciante, Phys. Rev. D **103**, 044021 (2021). https://doi.org/10.1103/PhysRevD.103.044021. arXiv:2101.09242 [astro-ph.CO]
82. J. Ferreira, T. Barreiro, J. Mimoso, N.J. Nunes, Phys. Rev. D **105**, 123531 (2022). https://doi.org/10.1103/PhysRevD.105.123531. arXiv:2203.13788 [astro-ph.CO]
83. G.N. Gadbail, S. Mandal, P.K. Sahoo, Phys. Lett. B **835**, 137509 (2022). https://doi.org/10.1016/j.physletb.2022.137509. arXiv:2210.09237 [gr-qc]
84. P. Sarmah, U.D. Goswami, Phys. Dark Univ. **46**, 101556 (2024). https://doi.org/10.1016/j.dark.2024.101556. arXiv:2403.16118 [gr-qc]
85. A.S. Agrawal, B. Mishra, P.K. Agrawal, Eur. Phys. J. C **83**, 113 (2023). https://doi.org/10.1140/epjc/s10052-023-11266-8. arXiv:2206.02783 [gr-qc]
86. S.A. Narawade, S.H. Shekh, B. Mishra, W. Khyllep, J. Dutta, (2023). arXiv:2303.01985 [gr-qc]
87. H. Shabani, A. De, T.-H. Loo, Eur. Phys. J. C **83**, 535 (2023). https://doi.org/10.1140/epjc/s10052-023-11722-5. arXiv:2304.02949 [gr-qc]
88. G.G.L. Nashed, Fortsch. Phys. **72**, 2400037 (2024). https://doi.org/10.1002/prop.202400037
89. S.K. Maurya, K. Newton Singh, S.V. Lohakare, B. Mishra, Fortsch. Phys. **70**, 2200061 (2022). https://doi.org/10.1002/prop.202200061. arXiv:2208.04735 [gr-qc]
90. S.A. Narawade, S.P. Singh, B. Mishra, Phys. Dark Univ. **42**, 101282 (2023). https://doi.org/10.1016/j.dark.2023.101282. arXiv:2303.06427 [gr-qc]
91. S. Mandal, P.K. Sahoo, J.R.L. Santos, Phys. Rev. D **102**, 024057 (2020). https://doi.org/10.1103/PhysRevD.102.024057. arXiv:2008.01563 [gr-qc]
92. G. Subramaniam, A. De, T.-H. Loo, Y.K. Goh, Fortsch. Phys. **71**, 2300038 (2023). https://doi.org/10.1002/prop.202300038. arXiv:2304.02300 [gr-qc]
93. L. Järv, M. Rünkla, M. Saal, O. Vilson, Phys. Rev. D **97**, 124025 (2018). https://doi.org/10.1103/PhysRevD.97.124025. arXiv:1802.00492 [gr-qc]
94. J.V. Cunha, J.A.S. Lima, Mon. Not. R. Astron. Soc. **390**, 210 (2008). https://doi.org/10.1111/j.1365-2966.2008.13640.x. arXiv:0805.1261 [astro-ph]
95. J.V. Cunha, Phys. Rev. D **79**, 047301 (2009). https://doi.org/10.1103/PhysRevD.79.047301. arXiv:0811.2379 [astro-ph]
96. R. Nair, S. Jhingan, D. Jain, JCAP **01**, 018 (2012). https://doi.org/10.1088/1475-7516/2012/01/018. arXiv:1109.4574 [astro-ph.CO]
97. A.A. Mamon, S. Das, Eur. Phys. J. C **77**, 495 (2017). https://doi.org/10.1140/epjc/s10052-017-5066-4. arXiv:1610.07337 [gr-qc]
98. A.G. Riess et al. (Supernova Search Team), Astrophys. J. **607**, 665 (2004). https://doi.org/10.1086/383612. arXiv:astro-ph/0402512
99. A.A. Mamon, Mod. Phys. Lett. A **33**, 1850056 (2018). https://doi.org/10.1142/S0217732318500566. arXiv:1702.04916 [gr-qc]
100. A. Shafieloo, Mon. Not. R. Astron. Soc. **380**, 1573 (2007). https://doi.org/10.1111/j.1365-2966.2007.12175.x. arXiv:astro-ph/0703034
101. T. Holsclaw, U. Alam, B. Sanso, H. Lee, K. Heitmann, S. Habib, D. Higdon, Phys. Rev. D **84**, 083501 (2011). https://doi.org/10.1103/PhysRevD.84.083501. arXiv:1104.2041 [astro-ph.CO]
102. B. Santos, J.C. Carvalho, J.S. Alcaniz, Astropart. Phys. **35**, 17 (2011). https://doi.org/10.1016/j.astropartphys.2011.04.002. arXiv:1009.2733 [astro-ph.CO]
103. T. Holsclaw, U. Alam, B. Sanso, H. Lee, K. Heitmann, S. Habib, D. Higdon, Phys. Rev. D **82**, 103502 (2010). https://doi.org/10.1103/PhysRevD.82.103502. arXiv:1009.5443 [astro-ph.CO]
104. R.G. Crittenden, G.-B. Zhao, L. Pogosian, L. Samushia, X. Zhang, JCAP **02**, 048 (2012). https://doi.org/10.1088/1475-7516/2012/02/048. arXiv:1112.1693 [astro-ph.CO]
105. R. Nair, S. Jhingan, D. Jain, JCAP **01**, 005 (2014). https://doi.org/10.1088/1475-7516/2014/01/005. arXiv:1306.0606 [astro-ph.CO]
106. V. Sahni, A. Starobinsky, Int. J. Mod. Phys. D **15**, 2105 (2006). https://doi.org/10.1142/S0218271806009704. arXiv:astro-ph/0610026

107. S. Chatzidakis, A. Giacomini, P.G.L. Leach, G. Leon, A. Paliathanasis, S. Pan, JHEAp **36**, 141 (2022). https://doi.org/10.1016/j.jheap.2022.10.001. arXiv:2206.06639 [gr-qc]
108. E. Di Valentino, A. Melchiorri, J. Silk, Nat. Astron. **4**, 196 (2019). https://doi.org/10.1038/s41550-019-0906-9. arXiv:1911.02087 [astro-ph.CO]
109. W. Yang, W. Giarè, S. Pan, E. Di Valentino, A. Melchiorri, J. Silk, Phys. Rev. D **107**, 063509 (2023). https://doi.org/10.1103/PhysRevD.107.063509. arXiv:2210.09865 [astro-ph.CO]
110. S. Vagnozzi, E. Di Valentino, S. Gariazzo, A. Melchiorri, O. Mena, J. Silk, Phys. Dark Univ. **33**, 100851 (2021). https://doi.org/10.1016/j.dark.2021.100851. arXiv:2010.02230 [astro-ph.CO]
111. S. Vagnozzi, A. Loeb, M. Moresco, Astrophys. J. **908**, 84 (2021). https://doi.org/10.3847/1538-4357/abd4df. arXiv:2011.11645 [astro-ph.CO]
112. M. Cruz, S. Lepe, Class. Quantum Gravity **35**, 155013 (2018). https://doi.org/10.1088/1361-6382/aacd9e. arXiv:1802.00097 [gr-qc]
113. S. Dhawan, J. Alsing, S. Vagnozzi, Mon. Not. R. Astron. Soc. **506**, L1 (2021). https://doi.org/10.1093/mnrasl/slab058. arXiv:2104.02485 [astro-ph.CO]
114. Y. Lai, C. Howlett, T.M. Davis, Mon. Not. R. Astron. Soc. **518**, 1840 (2022). https://doi.org/10.1093/mnras/stac3252. arXiv:2209.04166 [astro-ph.CO]
115. N. Dimakis, A. Paliathanasis, M. Roumeliotis, T. Christodoulakis, Phys. Rev. D **106**, 043509 (2022). https://doi.org/10.1103/PhysRevD.106.043509. arXiv:2205.04680 [gr-qc]
116. F.K. Anagnostopoulos, V. Gakis, E.N. Saridakis, S. Basilakos, Eur. Phys. J. C **83**, 58 (2023). https://doi.org/10.1140/epjc/s10052-023-11190-x. arXiv:2205.11445 [gr-qc]
117. A. Mukherjee, Mon. Not. R. Astron. Soc. **460**, 273 (2016). https://doi.org/10.1093/mnras/stw964. arXiv:1605.08184 [astro-ph.CO]
118. P.A.R. Ade et al. (Planck), Astron. Astrophys. **594**, A13 (2016). https://doi.org/10.1051/0004-6361/201525830. arXiv:1502.01589 [astro-ph.CO]
119. S. Nesseris, S. Basilakos, E.N. Saridakis, L. Perivolaropoulos, Phys. Rev. D **88**, 103010 (2013). https://doi.org/10.1103/PhysRevD.88.103010. arXiv:1308.6142 [astro-ph.CO]
120. E. Di Valentino, A. Melchiorri, J. Silk, Phys. Rev. D **92**, 121302 (2015). https://doi.org/10.1103/PhysRevD.92.121302. arXiv:1507.06646 [astro-ph.CO]
121. E. Di Valentino, A. Melchiorri, J. Silk, Phys. Lett. B **761**, 242 (2016). https://doi.org/10.1016/j.physletb.2016.08.043. arXiv:1606.00634 [astro-ph.CO]
122. G.-B. Zhao et al., Nat. Astron. **1**, 627 (2017). https://doi.org/10.1038/s41550-017-0216-z. arXiv:1701.08165 [astro-ph.CO]
123. E.M. Barboza Jr., J.S. Alcaniz, Phys. Lett. B **666**, 415 (2008). https://doi.org/10.1016/j.physletb.2008.08.012. arXiv:0805.1713 [astro-ph]
124. A. Al Mamon, S. Das, Int. J. Mod. Phys. D **25**, 1650032 (2016). https://doi.org/10.1142/S0218271816500322. arXiv:1507.00531 [gr-qc]